A BOUNDARY ELEMENT METHOD FOR CLASSICAL PLATE THEORY

by
Stephen V. Harren
http://www.harren.us

CONTENTS

0. Forword 1
1. Governing Equations of Classical Plate Theory 2
2. Governing Equations in Polar Coordinates 3
3. Unit Point Moment in the x–direction on an Infinite Plate 3
4. Unit Point Moment in the y–direction on an Infinite Plate 4
5. Unit Point Force in the z–direction on an Infinite Plate 5
6. The Moment Green's Functions 6
7. The Transverse Green's Function 8
8. The Moment Reciprocal Theorem 9
9. The Transverse Reciprocal Theorem 11
10. Gradients of the Transverse Reciprocal Theorem 12
11. Gradients of the Transverse Green's Function 12
12. Governing Equations on the Plate Boundary in the Curvilinear nt–system 14
13. Example – Bubble Distributed Load on a Rectangular Plate 16
14. Example – Sinusoidal Transverse Edge Load on an Annular Cantilever Plate 17
15. A 14-degree-of-freedom Curved Boundary Element 19
16. Boundary Solution via the Boundary Element Method 22
17. Calculation of Boundary Tensorial Quantities from the Boundary Solution 25
18. Calculation of Interior Tensorial Quantities from the Boundary Solution 26
19. Alternate Calculation of the Shear Vector 26
20. Numerical Example – Bubble Distributed Load on a Rectangular Plate 28
21. Numerical Example – Sinusoidal Transverse Edge Load on an Annular Cantilever Plate 32
22. Closing Comments 37

0. Foreword

Contained herein is work started by the author during the Global Pandemic of 2020. The reader will note that no references are given within. This is because the author is self-taught, and has no (or little) access to any university-level journals or publications. Nevertheless, the mathematical notation used herein is that contained in the text Introduction to the Mechanics of a Continuous Medium, by Lawrence E. Malvern, Prentice-Hall, Englewood Cliffs, NJ (1969). The basics of classical plate theory, although not in modern tensorial notation, can be found in the text Theory of Plates and Shells, by S. Timoshenko and S. Woinowsky-Krieger, McGraw-Hill, New York, NY (1959).

1. Governing Equations of Classical Plate Theory

In the Cartesian indicial equations for plate theory, the two-dimensional alternating symbol

$$\varepsilon_{ij} = \begin{bmatrix} 0 & 1 \\ -1 & 0 \end{bmatrix} \tag{1}$$

occurs. Note that $\boldsymbol{\varepsilon}^T = -\boldsymbol{\varepsilon}$, $\varepsilon_{ji}\varepsilon_{jk} = \varepsilon_{ij}\varepsilon_{kj} = \delta_{ik}$, and $\varepsilon_{ij}\varepsilon_{jk} = \varepsilon_{ji}\varepsilon_{kj} = -\delta_{ik}$, where δ_{ij} is the Kronecker delta, *i.e.,* the components of the two-dimensional identity matrix. The rotation vector ϕ_i and the curvatures κ_{ij} are given by

$$\phi_i = \varepsilon_{ij}u_{,j} \text{ or } \phi_x = u_{,y} \text{ and } \phi_y = -u_{,x}\,, \qquad \kappa_{ij} = u_{,ij}\,, \tag{2}$$

where u is the transverse displacement of the plate, and the comma denotes differentiation with respect to the spatial coordinates.

Hooke's Law for the plate is

$$M_{xx} = -M_{yy} = \frac{Eh^3}{12(1+\nu)}\,\kappa_{xy}\,, \qquad M_{xy} = -\frac{Eh^3}{12(1-\nu^2)}\left(\kappa_{xx} + \nu\kappa_{yy}\right),$$
$$M_{yx} = \frac{Eh^3}{12(1-\nu^2)}\left(\nu\kappa_{xx} + \kappa_{yy}\right), \tag{3}$$

where M_{ij} are the components of the moment tensor, E is Young's modulus, ν is Poisson's ratio, and h is the (transverse) thickness of the plate. The quantity M_{ij} is the moment vector acting on the i–face pointing in the j–direction. Thus, for a surface with outward-pointing unit normal $\mathbf{n}$, the moment vector $\boldsymbol{\mathcal{M}}$ acting on that surface is $\mathcal{M}_j = n_i M_{ij}$. In any case, eqns. (3) can be written in tensorial form as

$$M_{im}\varepsilon_{mj} = (\mathbf{M}\cdot\boldsymbol{\varepsilon})_{ij} = L_{ijkl}\kappa_{kl}\,, \qquad L_{ijkl} = \frac{Eh^3}{12(1-\nu^2)}\left[(1-\nu)I_{ijkl} + \nu\delta_{ij}\delta_{kl}\right],$$
$$I_{ijkl} = \frac{1}{2}\left(\delta_{ik}\delta_{jl} + \delta_{jk}\delta_{il}\right). \tag{4}$$

Note that $\mathbf{L}$ possesses full symmetry, *i.e.,* $L_{ijkl} = L_{jikl} = L_{ijlk} = L_{klij}$.

The moment-equilibrium equations are

$$M_{ji,j} = -\varepsilon_{ij}V_j \text{ or } V_j = -\varepsilon_{ij}M_{ki,k}\,, \tag{5}$$

which, when written out, are $V_x = M_{xy,x} + M_{yy,y}$ and $V_y = -M_{xx,x} - M_{yx,y}$. In eqns. (5), V_i are the components of the internal transverse shear resultant vector. Now, substitution of the last of eqns. (2) and eqns. (4) into eqns. (5) gives the expression for the shear resultant components

$$V_i = -\frac{Eh^3}{12(1-\nu^2)}\left(\nabla^2 u\right)_{,i}\,, \tag{6}$$

where $\nabla^2 u = u_{,jj} = u_{,xx} + u_{,yy}$ is the Laplacian (or harmonic) of u. Written out, eqns. (6) are

$$V_x = -\frac{Eh^3}{12(1-\nu^2)}\left(u_{,xxx} + u_{,xyy}\right), \qquad V_y = -\frac{Eh^3}{12(1-\nu^2)}\left(u_{,xxy} + u_{,yyy}\right). \tag{7}$$

Now, transverse force-equilibrium is

$$V_{i,i} + q = 0\,, \tag{8}$$

where q is the distributed load, *i.e.,* force per unit area of plate, with positive being in the positive (transverse) z–direction. Finally, substitution of eqn. (6) into eqn. (8) gives the governing equation of the plate, *viz.,*

$$\frac{Eh^3}{12(1-\nu^2)}\,\nabla^4 u = q\,, \tag{9}$$

where $\nabla^4 u = u_{,iijj} = u_{,xxxx} + 2u_{,xxyy} + u_{,yyyy}$ is the bi-harmonic of u.

2. Governing Equations in Polar Coordinates

Here, the governing equations of **§1** are listed, without comment, in polar coordinates. The components of the rotation vector are

$$\phi_r = \frac{1}{r}u_{,\theta}\,, \qquad \phi_\theta = -u_{,r}\,. \tag{10}$$

The components of the curvature tensor are

$$\kappa_{rr} = u_{,rr}\,, \qquad \kappa_{\theta\theta} = \frac{1}{r^2}u_{,\theta\theta} + \frac{1}{r}u_{,r}\,, \qquad \kappa_{r\theta} = \kappa_{\theta r} = \frac{1}{r}u_{,r\theta} - \frac{1}{r^2}u_{,\theta}\,. \tag{11}$$

Hooke's Law is the same as eqns. (3), *i.e.,*

$$M_{rr} = -M_{\theta\theta} = \frac{Eh^3}{12(1+\nu)}\,\kappa_{r\theta}\,, \qquad M_{r\theta} = -\frac{Eh^3}{12(1-\nu^2)}\,(\kappa_{rr} + \nu\kappa_{\theta\theta})\,,$$
$$M_{\theta r} = \frac{Eh^3}{12(1-\nu^2)}\,(\nu\kappa_{rr} + \kappa_{\theta\theta})\,. \tag{12}$$

The moment-equilibrium equations are

$$M_{r\theta,r} + \frac{1}{r}M_{\theta\theta,\theta} + \frac{1}{r}\,(M_{r\theta} + M_{\theta r}) - V_r = 0\,,$$
$$M_{rr,r} + \frac{1}{r}M_{\theta r,\theta} + \frac{1}{r}\,(M_{rr} - M_{\theta\theta}) + V_\theta = 0\,, \tag{13}$$

and the expressions for the shear resultants are

$$V_r = -\frac{Eh^3}{12(1-\nu^2)}\left(u_{,rrr} + \frac{1}{r}u_{,rr} - \frac{1}{r^2}u_{,r} + \frac{1}{r^2}u_{,r\theta\theta} - \frac{2}{r^3}u_{,\theta\theta}\right),$$
$$V_\theta = -\frac{Eh^3}{12(1-\nu^2)}\left(\frac{1}{r}u_{,rr\theta} + \frac{1}{r^2}u_{,r\theta} + \frac{1}{r^3}u_{,\theta\theta\theta}\right). \tag{14}$$

Finally, the bi-harmonic operator in eqn. (9) is

$$\nabla^4 u = u_{,rrrr} + \frac{2}{r}u_{,rrr} - \frac{1}{r^2}u_{,rr} + \frac{2}{r^2}u_{,rr\theta\theta} + \frac{1}{r^3}u_{,r} - \frac{2}{r^3}u_{,r\theta\theta} + \frac{4}{r^4}u_{,\theta\theta} + \frac{1}{r^4}u_{,\theta\theta\theta\theta}\,. \tag{15}$$

3. Unit Point Moment in the x–direction on an Infinite Plate

Figure 1 below depicts a unit point moment vector applied at the origin of an infinite plate. The sense of the twist is given by the so-called right-hand rule. Here, one assumes a displacement of the form

$$u = f(r)\sin\theta\,. \tag{16}$$

Substituting eqn. (16) into $\nabla^4 u = 0$ *cf.,* eqn. (15), one obtains

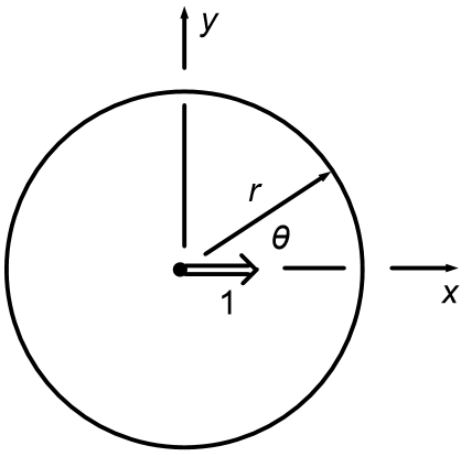

Figure 1. A unit point moment applied at the origin of an infinite plate.

$$f'''' + \frac{2}{r} f''' - \frac{3}{r^2} f'' + \frac{3}{r^3} f' - \frac{3}{r^4} f = 0\,, \qquad (17)$$

which has four independent solutions. The one of interest is $f(r) = kr \ln r$ so that

$$u = kr \ln r \sin\theta \qquad (18)$$

where the value of the constant k is to be determined. Equations (11) and (18) yield the curvatures

$$\kappa_{rr} = \kappa_{\theta\theta} = k \frac{\sin\theta}{r}\,, \qquad \kappa_{r\theta} = k \frac{\cos\theta}{r} \qquad (19)$$

so that via eqns. (12), the moments are

$$M_{rr} = -M_{\theta\theta} = \frac{Eh^3}{12(1+\nu)}\, k \frac{\cos\theta}{r}\,, \qquad M_{r\theta} = -M_{\theta r} = -\frac{Eh^3}{12(1-\nu)}\, k \frac{\sin\theta}{r}\,. \qquad (20)$$

Now, the moment vector acting on the outer surface of the circle in Fig. 1 is $\boldsymbol{\mathcal{M}} = M_{rr}\mathbf{e}_r + M_{r\theta}\mathbf{e}_\theta$, where $\mathbf{e}_r = \cos\theta\, \mathbf{e}_x + \sin\theta\, \mathbf{e}_y$ and $\mathbf{e}_\theta = -\sin\theta\, \mathbf{e}_x + \cos\theta\, \mathbf{e}_y$ are the polar coordinate base vectors, and $\mathbf{e}_x$ and $\mathbf{e}_y$ are the Cartesian base vectors. The moment vector is then $\boldsymbol{\mathcal{M}} = \mathcal{M}_x \mathbf{e}_x + \mathcal{M}_y \mathbf{e}_y$, with

$$\mathcal{M}_x = \frac{Eh^3}{12(1-\nu^2)} \frac{k}{r} \left[(1-\nu)\cos^2\theta + (1+\nu)\sin^2\theta \right],$$

$$\mathcal{M}_y = -\frac{\nu E h^3}{6(1-\nu^2)} \frac{k}{r} \sin\theta\cos\theta\,. \qquad (21)$$

Next, enforcing that

$$\int_0^{2\pi} \mathcal{M}_x r \mathrm{d}\theta = -1 \qquad \Rightarrow \qquad k = -\frac{6(1-\nu^2)}{\pi E h^3}\,. \qquad (22)$$

Also, note that

$$\int_0^{2\pi} \mathcal{M}_y r \mathrm{d}\theta = 0 \qquad (23)$$

is satisfied identically. Notwithstanding, finally, eqns. (18), (22) and $y = r\sin\theta$ give the displacement for this problem, *viz.,*

$$u = -\frac{6(1-\nu^2)}{\pi E h^3}\, y \ln r\,. \qquad (24)$$

4. Unit Point Moment in the y–direction on an Infinite Plate

Here, at the origin, the unit point moment vector points in the y–direction, as is pictured below in Fig. 2. By inspection, looking at eqn. (24), the displacement is

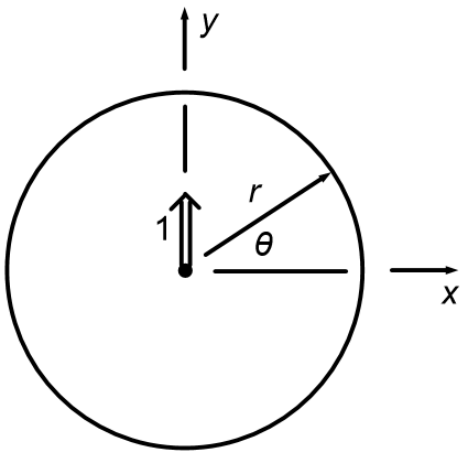

Figure 2. A unit point moment applied at the origin of an infinite plate.

$$u = \frac{6(1-\nu^2)}{\pi E h^3}\, x \ln r \,. \tag{25}$$

Now, using $r = \sqrt{x^2 + y^2}$, one sees that

$$r_{,x} = \frac{x}{r}\,, \qquad r_{,y} = \frac{y}{r}\,. \tag{26}$$

Via the last of eqns. (2), eqns. (3), eqn. (25) and eqns. (26), the moment components are obtained as

$$M_{xx} = -M_{yy} = \frac{(1-\nu)}{2\pi}\left[\frac{y}{r^2} - 2\frac{x^2 y}{r^4}\right],$$

$$M_{xy} = -\frac{1}{2\pi}\left[(3+\nu)\frac{x}{r^2} - 2\frac{x^3}{r^4} - 2\nu\frac{xy^2}{r^4}\right],$$

$$M_{yx} = \frac{1}{2\pi}\left[(1+3\nu)\frac{x}{r^2} - 2\nu\frac{x^3}{r^4} - 2\frac{xy^2}{r^4}\right]. \tag{27}$$

Differentiating the moments (27), by way of eqns. (5), yields the shear components

$$V_x = -\frac{1}{\pi}\left(\frac{1}{r^2} - 2\frac{x^2}{r^4}\right), \qquad V_y = \frac{2}{\pi}\frac{xy}{r^4}\,. \tag{28}$$

Finally, one may verify that eqns. (28) satisfy eqn. (8), *i.e.,*

$$V_{x,x} + V_{y,y} = 0 \tag{29}$$

so that equilibrium is satisfied.

To show that this solution corresponds to Fig. 2, evaluate the moment vector on the outer surface of the circle in Fig. 2. The outward-pointing unit normal there is $\mathbf{n} = \mathbf{e}_r = \cos\theta\, \mathbf{e}_x + \sin\theta\, \mathbf{e}_y$, and then the components of the moment vector are $\mathcal{M}_j = n_i M_{ij}$, or by using $x = r\cos\theta$ and $y = r\sin\theta$ in eqns. (27), one has

$$\mathcal{M}_x = \frac{\nu}{\pi r}\sin\theta\cos\theta\,, \qquad \mathcal{M}_y = -\frac{1}{2\pi r}\left[\,(1+\nu)\cos^2\theta + (1-\nu)\sin^2\theta\,\right]. \tag{30}$$

Equations (30) satisfy

$$\int_0^{2\pi} \mathcal{M}_x r\mathrm{d}\theta = 0 \;\text{ and }\; \int_0^{2\pi} \mathcal{M}_y r\mathrm{d}\theta = -1 \tag{31}$$

as desired.

5. Unit Point Force in the *z*–direction on an Infinite Plate

Figure 3 shows a unit point force applied at the origin of an infinite plate. The force acts in the positive z–direction. Here we assume that the displacement depends only on r, *i.e.,* $u = u(r)$. In this case, the biharmonic equation (15) reduces to

$$u'''' + \frac{2}{r}u''' - \frac{1}{r^2}u'' + \frac{1}{r^3}u' = 0\,, \tag{32}$$

which has four independent solutions. The one of interest is

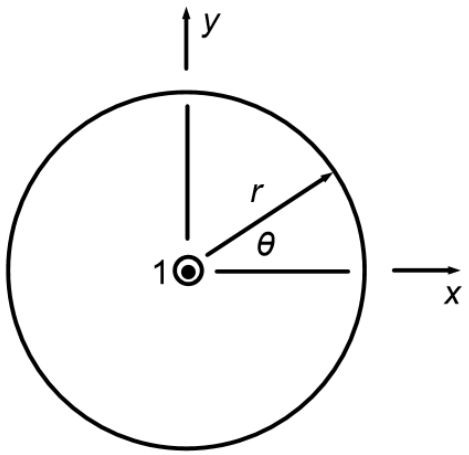

Figure 3. Unit point force applied at the origin of an infinite plate. The force acts in the positive z–direction.

$$u = kr^2 \ln r \,, \tag{33}$$

where the value of the constant k is to be determined. From eqns. (11), the curvatures are

$$\kappa_{rr} = u'' = k(2\ln r + 3)\,,$$
$$\kappa_{\theta\theta} = \frac{1}{r}u' = k(2\ln r + 1)\,, \tag{34}$$
$$\kappa_{r\theta} = \kappa_{\theta r} = 0\,.$$

Next, eqns. (12) give the moments

$$M_{r\theta} = -\frac{Eh^3}{12(1-\nu^2)}\, k\,[\,(3+\nu) + 2(1+\nu)\ln r\,]\,,$$
$$M_{\theta r} = \frac{Eh^3}{12(1-\nu^2)}\, k\,[\,(1+3\nu) + 2(1+\nu)\ln r\,]\,, \tag{35}$$
$$M_{rr} = -M_{\theta\theta} = 0\,.$$

Equations (14) then give the internal shear vector

$$V_r = -\frac{Eh^3}{12(1-\nu^2)}\left(u''' + \frac{1}{r}u'' - \frac{1}{r^2}u'\right) = -\frac{Eh^3}{3(1-\nu^2)}\,\frac{k}{r}\,, \qquad V_\theta = 0\,. \tag{36}$$

On the outer surface of the circle in Fig. 3, enforcing

$$\int_0^{2\pi} V_r r\,\mathrm{d}\theta = -1 \qquad \Rightarrow \qquad k = \frac{3(1-\nu^2)}{2\pi E h^3} \tag{37}$$

so that the displacement which solves this problem is

$$u = \frac{3(1-\nu^2)}{2\pi E h^3}\, r^2 \ln r\,. \tag{38}$$

6. The Moment Green's Functions

Translate the solutions in **§3** and **§4** by $\mathbf{x}^0$ so that the point moment vectors are applied at point $\mathbf{x}^0$. Also, introduce the notation

$$X_i = x_i - x_i^0\,, \qquad r = \sqrt{X^2 + Y^2} \tag{39}$$

where $X_1 \equiv X$ and $X_2 \equiv Y$. Note that

$$r_{,i} = \frac{X_i}{r}\,, \tag{40}$$

where, again, the comma indicates differentiation with respect to x_i. In any case, let u^k denote the displacement due to a unit point moment vector in the k–direction. Then, from eqns. (24) and (25),

$$u^k = -\frac{6(1-\nu^2)}{\pi E h^3}\,\varepsilon_{kj} X_j \ln r\,. \tag{41}$$

Using eqn. (41) in the first of eqns. (2) gives the rotations

$$\phi_l^k = -\frac{6(1-\nu^2)}{\pi E h^3}\left(\delta_{lk}\ln r + \varepsilon_{li}\varepsilon_{kj}\frac{X_i X_j}{r^2}\right), \tag{42}$$

and the last of eqns. (2) gives the curvatures

$$\kappa_{ij}^k = -\frac{6(1-\nu^2)}{\pi E h^3}\,\varepsilon_{kp}\left(\frac{\delta_{ip}X_j + \delta_{pj}X_i + \delta_{ij}X_p}{r^2} - 2\frac{X_p X_i X_j}{r^4}\right). \tag{43}$$

Next, substitution of eqn. (43) into eqn. (4) yields the moment field

$$M_{iq}^k = -\frac{1}{2\pi}\,\varepsilon_{kp}\left[(1-\nu)\varepsilon_{qj}\left\{\frac{\delta_{ip}X_j + \delta_{pj}X_i + \delta_{ij}X_p}{r^2} - 2\frac{X_p X_i X_j}{r^4}\right\} + 2\nu\varepsilon_{qi}\frac{X_p}{r^2}\right], \tag{44}$$

Finally, differentiate eqn. (44) via eqn. (5) to obtain the internal shear vector

$$V_l^k = \frac{1}{\pi}\,\varepsilon_{kp}\left(\delta_{lp}\frac{1}{r^2} - 2\frac{X_p X_l}{r^4}\right). \tag{45}$$

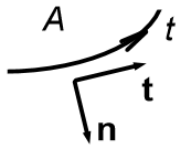

Figure 4. A portion of the plate boundary as described in the text.

Some of the quantities needed for implementing the Boundary Element Method are in the nt–system of the plate boundary, which system is shown at left. The domain of the plate is A, and the t–coordinate is arc length along the plate's boundary measured in the counterclockwise sense. The outward-pointing unit normal vector is **n**, and the unit tangent vector is **t**. Notwithstanding, the relations

$$\varepsilon_{ij}t_j = n_i\,, \qquad \varepsilon_{ij}n_i = t_j \tag{46}$$

have been used in calculating the expressions below.

The tangential rotation component is, from eqn. (42),

$$\phi_t^k = t_l\phi_l^k = -\frac{6(1-\nu^2)}{\pi E h^3}\left(t_k\ln r - n_i\varepsilon_{kj}\frac{X_i X_j}{r^2}\right). \tag{47}$$

Using eqn. (44), on the boundary, the moment vector components are,

$$\mathcal{M}_n^k = n_i M_{ij}^k n_j = -\frac{1}{2\pi}\,\varepsilon_{kp}(1-\nu)\left[\frac{n_p(\mathbf{t}\cdot\mathbf{X}) + t_p(\mathbf{n}\cdot\mathbf{X})}{r^2} - 2(\mathbf{n}\cdot\mathbf{X})(\mathbf{t}\cdot\mathbf{X})\frac{X_p}{r^4}\right],$$

$$\mathcal{M}_t^k = n_i M_{ij}^k t_j = \frac{1}{2\pi}\,\varepsilon_{kp}\left[(1+\nu)\frac{X_p}{r^2} + 2(1-\nu)(\mathbf{n}\cdot\mathbf{X})\left\{\frac{n_p}{r^2} - (\mathbf{n}\cdot\mathbf{X})\frac{X_p}{r^4}\right\}\right], \tag{48}$$

where $\mathbf{n}\cdot\mathbf{X} = n_i X_i$, *etc.* Next, the normal component of the shear vector is, from eqn. (45),

$$V_n^k = n_i V_i^k = \frac{1}{\pi}\,\varepsilon_{kp}\left[\frac{n_p}{r^2} - 2(\mathbf{n}\cdot\mathbf{X})\frac{X_p}{r^4}\right]. \tag{49}$$

The quantity $\mathcal{M}_{n,t}^k$ is also required for the implementation of the Boundary Element Method. Consequently, the base vectors **n** and **t** need to be differentiated. Figure 5 below shows a portion of the plate's boundary, and the unit vectors there are written as

$$\mathbf{n} = \cos\alpha\,\mathbf{e}_x + \sin\alpha\,\mathbf{e}_y\,, \qquad \mathbf{t} = -\sin\alpha\,\mathbf{e}_x + \cos\alpha\,\mathbf{e}_y\,. \tag{50}$$

With eqns. (50) in part, one obtains the derivatives

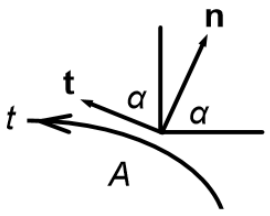

Figure 5. The nt–system unit vectors.

$$n_{i,t} = t_i\alpha_{,t}\,, \qquad t_{i,t} = -n_i\alpha_{,t}\,, \qquad X_{i,t} = x_{i,t} \equiv t_i\,,$$
$$r_{,t} = \frac{\mathbf{t}\cdot\mathbf{X}}{r}\,, \tag{51}$$
$$(\mathbf{t}\cdot\mathbf{X})_{,t} = 1 - (\mathbf{n}\cdot\mathbf{X})\alpha_{,t}\,, \qquad (\mathbf{n}\cdot\mathbf{X})_{,t} = (\mathbf{t}\cdot\mathbf{X})\alpha_{,t}\,.$$

Differentiation of the first of eqns. (48) then yields

$$\mathcal{M}^k_{n,t} = -\frac{1}{2\pi}\,\varepsilon_{kp}(1-\nu)\left[\frac{n_p}{r^2} + 2\frac{t_p(\mathbf{t}\cdot\mathbf{X}) - n_p(\mathbf{n}\cdot\mathbf{X})}{r^2}\,\alpha_{,t}\right.$$
$$\left. -2\frac{(\mathbf{n}\cdot\mathbf{X})X_p + 2(\mathbf{n}\cdot\mathbf{X})(\mathbf{t}\cdot\mathbf{X})t_p + (\mathbf{t}\cdot\mathbf{X})^2 n_p}{r^4} + 2\frac{(\mathbf{n}\cdot\mathbf{X})^2 - (\mathbf{t}\cdot\mathbf{X})^2}{r^4}X_p\alpha_{,t} + 8\frac{(\mathbf{n}\cdot\mathbf{X})(\mathbf{t}\cdot\mathbf{X})^2 X_p}{r^6}\right]. \tag{52}$$

Finally, the Kirchhoff (or effective) shear force is constructed from eqns. (49) and (52), *viz.,*

$$\bar{V}^k_n = V^k_n - \mathcal{M}^k_{n,t}\,. \tag{53}$$

7. The Transverse Green's Function

Once again, translate the solution in **§5** by $\mathbf{x}^0$ so that the point force is applied at point $\mathbf{x}^0$. Equation (38) becomes

$$u^z = \frac{3(1-\nu^2)}{2\pi E h^3}\,r^2\ln r, \tag{54}$$

where the superscript z has been added to indicate that the unit point load is applied in the z–direction. Now, differentiate eqn. (54) via the first of eqns. (2) to obtain the rotation vector

$$\phi^z_j = \frac{3(1-\nu^2)}{2\pi E h^3}\,\varepsilon_{ji}\,(2\ln r + 1)X_i\,, \tag{55}$$

where the notation of eqns. (39) is used. Next, eqn. (54) and the last of eqns. (2) give the curvatures

$$\kappa^z_{ij} = \frac{3(1-\nu^2)}{2\pi E h^3}\left[(2\ln r + 1)\delta_{ij} + 2\frac{X_iX_j}{r^2}\right], \tag{56}$$

and then substitution of eqn. (56) into Hooke's Law (4) yields the moment tensor

$$M^z_{ip} = \frac{1}{8\pi}\left\{[\,(1+3\nu) + 2(1+\nu)\ln r\,]\varepsilon_{pi} + 2(1-\nu)\varepsilon_{pj}\frac{X_iX_j}{r^2}\right\}. \tag{57}$$

Finally, differentiating eqn. (57) via eqns. (5), one finds the internal shear vector

$$V^z_i = -\frac{1}{2\pi}\,\frac{X_i}{r^2}\,. \tag{58}$$

Now, for the required quantities in the boundary nt–system, eqn. (55) gives

$$\phi^z_t = t_i\phi^z_i = -\frac{3(1-\nu^2)}{2\pi E h^3}\,(\mathbf{n}\cdot\mathbf{X})(2\ln r + 1) \tag{59}$$

for the tangential rotation. The boundary moment vector $\boldsymbol{\mathcal{M}}^z$ in the nt–system is

$$\mathcal{M}_n^z = n_i M_{ij}^z n_j = \frac{1}{4\pi}(1-\nu)(\mathbf{n}\cdot\mathbf{X})(\mathbf{t}\cdot\mathbf{X})\frac{1}{r^2},$$
$$\mathcal{M}_t^z = n_i M_{ij}^z t_j = -\frac{1}{8\pi}\left[(1+3\nu)+2(1+\nu)\ln r + 2(1-\nu)(\mathbf{n}\cdot\mathbf{X})^2\frac{1}{r^2}\right], \tag{60}$$

which are obtained from eqn. (57). The normal component of the shear vector follows from eqn. (58), *viz.,*

$$V_n^z = n_i V_i^z = -\frac{1}{2\pi}(\mathbf{n}\cdot\mathbf{X})\frac{1}{r^2}. \tag{61}$$

Using the technique of **§6**, differentiation of the first of eqns. (60) gives

$$\mathcal{M}_{n,t}^z = \frac{1}{4\pi}(1-\nu)\left[\frac{(\mathbf{n}\cdot\mathbf{X})}{r^2} + \frac{(\mathbf{t}\cdot\mathbf{X})^2-(\mathbf{n}\cdot\mathbf{X})^2}{r^2}\alpha_{,t} - 2\frac{(\mathbf{t}\cdot\mathbf{X})^2(\mathbf{n}\cdot\mathbf{X})}{r^4}\right]. \tag{62}$$

Finally, then, the Kirchhoff shear force follows from eqns. (61) and (62). Thus,

$$\bar{V}_n^z = V_n^z - \mathcal{M}_{n,t}^z. \tag{63}$$

8. The Moment Reciprocal Theorem

The Moment Green's Functions (MGFs) of **§6** satisfy moment-equilibrium, *i.e.,* $M_{ji,j}^k + \varepsilon_{ij}V_j^k = 0$. Multiply this equation by a (non-singular) rotation vector to obtain

$$\phi_i M_{ji,j}^k + \phi_i \varepsilon_{ij} V_j^k = 0. \tag{64}$$

Now, $\phi_i\varepsilon_{ij} = \varepsilon_{ij}\varepsilon_{il}u_{,l} = \delta_{jl}u_{,l} = u_{,j}$, where u is the corresponding (non-singular) displacement, so that eqn. (64) becomes

$$\phi_i M_{ji,j}^k + u_{,j}V_j^k = 0. \tag{65}$$

The product rule of differentiation gives $\left(uV_j^k\right)_{,j} = u_{,j}V_j^k + uV_{j,j}^k = u_{,j}V_j^k$ (since $V_{j,j}^k = 0$) so that eqn. (65) becomes

$$\phi_i M_{ji,j}^k + \left(uV_j^k\right)_{,j} = 0. \tag{66}$$

The product rule of differentiation also gives

$$\phi_i M_{ji,j}^k = \left(\phi_i M_{ji}^k\right)_{,j} - \phi_{i,j}M_{ji}^k. \tag{67}$$

Next, $\phi_{i,j}M_{ji}^k = \varepsilon_{il}u_{,lj}M_{ji}^k = \kappa_{lj}\left(\mathbf{M}^k\cdot\boldsymbol{\varepsilon}\right)_{jl} = \kappa_{lj}L_{jlpq}\kappa_{qp}^k = (\mathbf{M}\cdot\boldsymbol{\varepsilon})_{pq}\kappa_{qp}^k = M_{pm}\varepsilon_{mq}u_{,qp}^k = M_{pm}\phi_{m,p}^k$. With this result, eqn. (67) becomes

$$\phi_i M_{ji,j}^k = \left(\phi_i M_{ji}^k\right)_{,j} - M_{ji}\phi_{i,j}^k. \tag{68}$$

Substituting eqn. (68) into eqn. (66) then yields

$$\left(uV_j^k\right)_{,j} + \left(\phi_i M_{ji}^k\right)_{,j} = M_{ji}\phi_{i,j}^k. \tag{69}$$

Once again, using the product rule of differentiation,

$$\phi_{i,j}^k M_{ji} = \left(\phi_i^k M_{ji}\right)_{,j} - \phi_i^k M_{ji,j}. \tag{70}$$

With the moment-equilibrium equations $M_{ji,j} = -\varepsilon_{ij}V_j$ eqn. (70) is

$$\phi^k_{i,j}M_{ji} = \left(\phi^k_i M_{ji}\right)_{,j} + \phi^k_i \varepsilon_{ij} V_j \,. \tag{71}$$

Via $\phi^k_i \varepsilon_{ij} V_j = \varepsilon_{il} u^k_{,l} \varepsilon_{ij} V_j = \delta_{lj} u^k_{,l} V_j = u^k_{,j} V_j$, eqn. (71) is

$$\phi^k_{i,j}M_{ji} = \left(\phi^k_i M_{ji}\right)_{,j} + u^k_{,j} V_j \,. \tag{72}$$

For the fourth time, the product rule of differentiation shows $\left(u^k V_j\right)_{,j} = u^k_{,j} V_j + u^k V_{j,j}$, or from transverse equilibrium $V_{j,j} = -q$, eqn. (72) gives

$$\phi^k_{i,j}M_{ji} = \left(\phi^k_i M_{ji}\right)_{,j} + \left(u^k V_j\right)_{,j} + u^k q \,. \tag{73}$$

Equating eqns. (69) and (73), one finds

$$\left(u V^k_j\right)_{,j} + \left(\phi_i M^k_{ji}\right)_{,j} - \left(M_{ji}\phi^k_i\right)_{,j} - \left(V_j u^k\right)_{,j} = u^k q \,. \tag{74}$$

Finally, integrate eqn. (74) over the domain of the plate A, and use the Divergence Theorem on the terms on the left-hand eqn. (74) to obtain

$$\oint_t u V^k_n \mathrm{d}t + \oint_t \phi_i \mathcal{M}^k_i \mathrm{d}t - \oint_t \mathcal{M}_i \phi^k_i \mathrm{d}t - \oint_t V_n u^k \mathrm{d}t = \int_A u^k q \mathrm{d}A \,, \tag{75}$$

where $V^k_n = n_j V^k_j$, $\mathcal{M}^k_i = n_j M^k_{ji}$, $\mathcal{M}_i = n_j M_{ji}$ and $V_n = n_j V_j$.

Equation (75) is not quite the desired result since the boundary conditions for plate theory are in terms of ϕ_t and $\mathcal{M}_t$. Toward that end

$$\oint_t \phi^k_i \mathcal{M}_i \mathrm{d}t + \oint_t u^k V_n \mathrm{d}t = \oint_t \phi^k_t \mathcal{M}_t \mathrm{d}t + \oint_t \phi^k_n \mathcal{M}_n \mathrm{d}t + \oint_t u^k V_n \mathrm{d}t \,. \tag{76}$$

The product rule of differentiation, yet again, gives $\left(u^k \mathcal{M}_n\right)_{,t} = u^k_{,t} \mathcal{M}_n + u^k \mathcal{M}_{n,t} = \phi^k_n \mathcal{M}_n + u^k \mathcal{M}_{n,t}$ or $\mathrm{d}\left(u^k \mathcal{M}_n\right) = \phi^k_n \mathcal{M}_n \mathrm{d}t + u^k \mathcal{M}_{n,t} \mathrm{d}t$. Integrating this around the circuit gives

$$\oint_t \phi^k_n \mathcal{M}_n \mathrm{d}t = -\oint_t u^k \mathcal{M}_{n,t} \mathrm{d}t \,. \tag{77}$$

Substitution of eqn. (77) into eqn. (76) then gives

$$\oint_t \phi^k_i \mathcal{M}_i \mathrm{d}t + \oint_t u^k V_n \mathrm{d}t = \oint_t \phi^k_t \mathcal{M}_t \mathrm{d}t + \oint_t u^k \bar{V}_n \mathrm{d}t \,, \tag{78}$$

where $\bar{V}_n = V_n - \mathcal{M}_{n,t}$. Similarly,

$$\oint_t u V^k_n \mathrm{d}t + \oint_t \phi_i \mathcal{M}^k_i \mathrm{d}t = \oint_t u \bar{V}^k_n \mathrm{d}t + \oint_t \phi_t \mathcal{M}^k_t \mathrm{d}t \,, \tag{79}$$

where $\bar{V}^k_n = V^k_n - \mathcal{M}^k_{n,t}$. Putting eqns. (78) and (79) into eqn. (75) gives the Reciprocal Theorem, *i.e.,*

$$\oint_t u \bar{V}^k_n \mathrm{d}t + \oint_t \phi_t \mathcal{M}^k_t \mathrm{d}t - \oint_t \mathcal{M}_t \phi^k_t \mathrm{d}t - \oint_t \bar{V}_n u^k \mathrm{d}t = \int_A u^k q \mathrm{d}A \,. \tag{80}$$

9. The Transverse Reciprocal Theorem

The Transverse Green's Function (TGF) of **§7** satisfies moment-equilibrium, *i.e.*, $M^z_{ji,j} + \varepsilon_{ij} V^z_j = 0$. Multiply this equation by a (non-singular) rotation vector to obtain

$$\phi_i M^z_{ji,j} + \phi_i \varepsilon_{ij} V^z_j = 0, \tag{81}$$

or, by performing manipulations like those used to obtain eqn. (65) in **§8**,

$$\phi_i M^z_{ji,j} + u_{,j} V^z_j = 0\,. \tag{82}$$

From the product rule of differentiation, $\left(uV^z_j\right)_{,j} = u_{,j}V^z_j + uV^z_{j,j}$, which when substituted into eqn. (82) gives

$$\phi_i M^z_{ji,j} + \left(uV^z_j\right)_{,j} = uV^z_{j,j}\,. \tag{83}$$

Next, using the same procedure as was used to obtain eqns. (67) through (69) in **§8**, eqn. (83) becomes

$$\left(uV^z_j\right)_{,j} + \left(\phi_i M^z_{ji}\right)_{,j} - \phi^z_{i,j} M_{ji} = uV^z_{j,j}\,. \tag{84}$$

Here, the analog to eqn. (72) in **§8** is

$$\phi^z_{i,j} M_{ji} = \left(\phi^z_i M_{ji}\right)_{,j} + u^z_{,j} V_j\,. \tag{85}$$

Putting eqn. (85) into eqn. (84) yields

$$\left(uV^z_j\right)_{,j} + \left(\phi_i M^z_{ji}\right)_{,j} - \left(\phi^z_i M_{ji}\right)_{,j} - u^z_{,j} V_j = uV^z_{j,j}\,. \tag{86}$$

Via the product rule of differentiation again, $\left(u^z V_j\right)_{,j} = u^z_{,j}V_j + u^z V_{j,j} = u^z_{,j}V_j - u^z q$, where transverse equilibrium was used. Substituting this result into eqn. (86), one finds

$$\left(uV^z_j\right)_{,j} + \left(\phi_i M^z_{ji}\right)_{,j} - \left(M_{ji}\phi^z_i\right)_{,j} - \left(V_j u^z\right)_{,j} = uV^z_{j,j} + u^z q\,. \tag{87}$$

Now, integrate eqn. (87) over the domain of the plate A, and use the Divergence Theorem on the terms on the left-hand side of the equation. Thus,

$$\oint_t uV^z_n \mathrm{d}t + \oint_t \phi_i \mathcal{M}^z_i \mathrm{d}t - \oint_t \mathcal{M}_i \phi^z_i \mathrm{d}t - \oint_t V_n u^z \mathrm{d}t = \int_A uV^z_{j,j} \mathrm{d}A + \int_A u^z q \mathrm{d}A\,, \tag{88}$$

where $V^z_n = n_j V^z_j$, $\mathcal{M}^z_i = n_j M^z_{ji}$, $\mathcal{M}_i = n_j M_{ji}$ and $V_n = n_j V_j$.

For the transverse Green's function

$$\int_A V^z_{j,j} \mathrm{d}A = \oint_t V^z_n \mathrm{d}t = -\beta\,, \qquad \beta = \begin{bmatrix} 0 \text{ if } \mathbf{x}^0 \text{ is outside of } A \\ 1 \text{ if } \mathbf{x}^0 \text{ is in } A \end{bmatrix}. \tag{89}$$

Since $V^z_{j,j} = 0$ everywhere except at $\mathbf{x}^0$, where it is singular,

$$\int_A uV^z_{j,j} \mathrm{d}A = -\beta u(\mathbf{x}^0)\,. \tag{90}$$

Next, substitute eqn. (90) into eqn. (88) to obtain

$$\oint_t uV^z_n \mathrm{d}t + \oint_t \phi_i \mathcal{M}^z_i \mathrm{d}t - \oint_t \mathcal{M}_i \phi^z_i \mathrm{d}t - \oint_t V_n u^z \mathrm{d}t = \int_A u^z q \mathrm{d}A - \beta u(\mathbf{x}^0)\,. \tag{91}$$

Finally, following the procedure used to obtain eqns. (76) through (79) of **§8**, eqn. (91) yields the desired result

$$\oint_t u\bar{V}_n^z \mathrm{d}t + \oint_t \phi_t \mathcal{M}_t^z \mathrm{d}t - \oint_t \mathcal{M}_t \phi_t^z \mathrm{d}t - \oint_t \bar{V}_n u^z \mathrm{d}t = \int_A u^z q \mathrm{d}A - \beta u(\mathbf{x}^0) \,, \tag{92}$$

where $\bar{V}_n^z = V_n^z - \mathcal{M}_{n,t}^z$ and $\bar{V}_n = V_n - \mathcal{M}_{n,t}$.

10. Gradients of the Transverse Reciprocal Theorem

Looking at the case where the singularity $\mathbf{x}^0$ is inside the plate A, *i.e.,* $\beta = 1$, eqn. (92) becomes

$$u(\mathbf{x}^0) = -\oint_t u\bar{V}_n^z \mathrm{d}t - \oint_t \phi_t \mathcal{M}_t^z \mathrm{d}t + \oint_t \mathcal{M}_t \phi_t^z \mathrm{d}t + \oint_t \bar{V}_n u^z \mathrm{d}t + \int_A u^z q \mathrm{d}A \,. \tag{93}$$

If the plate quantities u, ϕ_t, $\mathcal{M}_t$ and $\bar{V}_n$ are known on the boundary, then eqn. (93) is a formula for the displacement in the interior A of the plate. Using the notation

$$f_{:i} = \frac{\partial f}{\partial x_i^0} \text{ and } \nabla_0^2 f = f_{:ii} \tag{94}$$

the derivatives of eqn. (93) with respect to $\mathbf{x}^0$ are

$$u_{:i}(\mathbf{x}^0) = -\oint_t u\bar{V}_{n:i}^z \mathrm{d}t - \oint_t \phi_t \mathcal{M}_{t:i}^z \mathrm{d}t + \oint_t \mathcal{M}_t \phi_{t:i}^z \mathrm{d}t + \oint_t \bar{V}_n u_{:i}^z \mathrm{d}t + \int_A u_{:i}^z q \mathrm{d}A \,. \tag{95}$$

The second derivatives are

$$u_{:ij}(\mathbf{x}^0) = -\oint_t u\bar{V}_{n:ij}^z \mathrm{d}t - \oint_t \phi_t \mathcal{M}_{t:ij}^z \mathrm{d}t + \oint_t \mathcal{M}_t \phi_{t:ij}^z \mathrm{d}t + \oint_t \bar{V}_n u_{:ij}^z \mathrm{d}t + \int_A u_{:ij}^z q \mathrm{d}A \,, \tag{96}$$

and the gradients of the Laplacian are

$$\nabla_0^2 u_{:i}(\mathbf{x}^0) = -\oint_t u\nabla_0^2 \bar{V}_{n:i}^z \mathrm{d}t - \oint_t \phi_t \nabla_0^2 \mathcal{M}_{t:i}^z \mathrm{d}t + \oint_t \mathcal{M}_t \nabla_0^2 \phi_{t:i}^z \mathrm{d}t + \oint_t \bar{V}_n \nabla_0^2 u_{:i}^z \mathrm{d}t + \int_A q\nabla_0^2 u_{:i}^z \mathrm{d}A \,. \tag{97}$$

From eqn. (95) the rotation vector ϕ_i can be found in the interior; from eqn. (96), the curvatures κ_{ij} and moments M_{ij}; and finally, from eqn. (97), the shear vector V_i.

11. Gradients of the Transverse Green's Function

To differentiate the quantities of the TGF in **§7** with respect to $\mathbf{x}^0$, so that the formulas in **§10** can be evaluated, one notes that

$$X_{i:j} = -\delta_{ij} \,, \qquad r_{:i} = -\frac{X_i}{r} \,, \qquad (\mathbf{n}\cdot\mathbf{X})_{:i} = -n_i \,, \qquad (\mathbf{t}\cdot\mathbf{X})_{:i} = -t_i \,. \tag{98}$$

The gradients of eqns. (54) and (59) are, respectively,

$$u_{:i}^z = -\frac{3(1-\nu^2)}{2\pi E h^3}(2\ln r + 1)X_i \tag{99}$$

and

$$\phi^z_{t:i} = \frac{3(1-\nu^2)}{2\pi E h^3}\left[\,(2\ln r + 1)n_i + 2(\mathbf{n}\cdot\mathbf{X})\frac{X_i}{r^2}\right]. \tag{100}$$

Again, respectively, the gradients of eqns. (60) through (63) are

$$\mathcal{M}^z_{t:i} = \frac{1}{4\pi}\left\{(1+\nu)\frac{X_i}{r^2} + 2(1-\nu)(\mathbf{n}\cdot\mathbf{X})\left[\frac{n_i}{r^2} - (\mathbf{n}\cdot\mathbf{X})\frac{X_i}{r^4}\right]\right\}, \tag{101}$$

$$V^z_{n:i} = \frac{1}{2\pi}\left[\frac{n_i}{r^2} - 2(\mathbf{n}\cdot\mathbf{X})\frac{X_i}{r^4}\right], \tag{102}$$

$$\begin{aligned}\mathcal{M}^z_{n,t:i} = \frac{1-\nu}{4\pi}\Bigg\{&-\frac{n_i}{r^2} + 2\left[\frac{(\mathbf{t}\cdot\mathbf{X})^2 n_i + 2(\mathbf{n}\cdot\mathbf{X})(\mathbf{t}\cdot\mathbf{X})t_i + (\mathbf{n}\cdot\mathbf{X})X_i}{r^4}\right]\\ &-8\frac{(\mathbf{n}\cdot\mathbf{X})(\mathbf{t}\cdot\mathbf{X})^2 X_i}{r^6} + 2\left[\frac{(\mathbf{n}\cdot\mathbf{X})n_i - (\mathbf{t}\cdot\mathbf{X})t_i}{r^2} + \frac{(\mathbf{t}\cdot\mathbf{X})^2 - (\mathbf{n}\cdot\mathbf{X})^2}{r^4}X_i\right]\alpha_{,t}\Bigg\},\end{aligned} \tag{103}$$

$$\bar{V}^z_{n:i} = V^z_{n:i} - \mathcal{M}^z_{n,t:i}\,. \tag{104}$$

The second gradients are, via differentiation of eqns. (99) through (104),

$$u^z_{:ij} = \frac{3(1-\nu^2)}{2\pi E h^3}\left[\,(2\ln r + 1)\delta_{ij} + 2\frac{X_i X_j}{r^2}\right], \tag{105}$$

$$\phi^z_{t:ij} = -\frac{3(1-\nu^2)}{\pi E h^3}\left[\frac{n_i X_j + X_i n_j + (\mathbf{n}\cdot\mathbf{X})\delta_{ij}}{r^2} - 2(\mathbf{n}\cdot\mathbf{X})\frac{X_i X_j}{r^4}\right], \tag{106}$$

$$\begin{aligned}\mathcal{M}^z_{t:ij} = \frac{1}{4\pi}\Bigg\{&(1+\nu)\left[-\frac{\delta_{ij}}{r^2} + 2\frac{X_i X_j}{r^4}\right] + 2(1-\nu)\Big[-\frac{n_i n_j}{r^2}\\ &+\frac{2(\mathbf{n}\cdot\mathbf{X})\big(n_i X_j + X_i n_j\big) + (\mathbf{n}\cdot\mathbf{X})^2\delta_{ij}}{r^4} - 4(\mathbf{n}\cdot\mathbf{X})^2\frac{X_i X_j}{r^6}\Big]\Bigg\},\end{aligned} \tag{107}$$

$$V^z_{n:ij} = \frac{1}{\pi}\left[\frac{n_i X_j + X_i n_j + (\mathbf{n}\cdot\mathbf{X})\delta_{ij}}{r^4} - 4(\mathbf{n}\cdot\mathbf{X})\frac{X_i X_j}{r^6}\right], \tag{108}$$

$$\begin{aligned}\mathcal{M}^z_{n,t:ij} = \frac{1-\nu}{2\pi}\Bigg\{&-\frac{2\left[\,(\mathbf{t}\cdot\mathbf{X})\big(n_i t_j + t_i n_j\big) + (\mathbf{n}\cdot\mathbf{X})t_i t_j\,\right] + \big(n_i X_j + X_i n_j\big) + (\mathbf{n}\cdot\mathbf{X})\delta_{ij}}{r^4}\\ &+4\frac{(\mathbf{t}\cdot\mathbf{X})^2\big(X_i n_j + n_i X_j\big) + 2(\mathbf{n}\cdot\mathbf{X})(\mathbf{t}\cdot\mathbf{X})\big(X_i t_j + t_i X_j\big) + (\mathbf{n}\cdot\mathbf{X})X_i X_j + (\mathbf{n}\cdot\mathbf{X})(\mathbf{t}\cdot\mathbf{X})^2\delta_{ij}}{r^6}\\ &-24(\mathbf{n}\cdot\mathbf{X})(\mathbf{t}\cdot\mathbf{X})^2\frac{X_i X_j}{r^8} + \Bigg[\frac{t_i t_j - n_i n_j}{r^2} + 4\frac{(\mathbf{t}\cdot\mathbf{X})^2 - (\mathbf{n}\cdot\mathbf{X})^2}{r^6}X_i X_j\\ &+\frac{2(\mathbf{n}\cdot\mathbf{X})\big(n_i X_j + X_i n_j\big) - 2(\mathbf{t}\cdot\mathbf{X})\big(t_i X_j + X_i t_j\big) + \{\,(\mathbf{n}\cdot\mathbf{X})^2 - (\mathbf{t}\cdot\mathbf{X})^2\,\}\delta_{ij}}{r^4}\Bigg]\alpha_{,t}\Bigg\},\end{aligned} \tag{109}$$

$$\bar{V}^z_{n:ij} = V^z_{n:ij} - \mathcal{M}^z_{n,t:ij}\,. \tag{110}$$

While this is an intermediate step, setting j to i in eqns. (105) through (110) yields the Laplacians

$$\nabla_0^2 u^z = \frac{6(1-\nu^2)}{\pi E h^3}\,(\ln r + 1)\,, \tag{111}$$

$$\nabla_0^2 \phi^z_t = -\frac{6(1-\nu^2)}{\pi E h^3}\,\frac{(\mathbf{n}\cdot\mathbf{X})}{r^2}\,, \tag{112}$$

$$\nabla_0^2 \mathcal{M}_t^z = \frac{1-\nu}{2\pi}\left[-\frac{1}{r^2}+2\frac{(\mathbf{n}\cdot\mathbf{X})^2}{r^4}\right], \tag{113}$$

$$\nabla_0^2 V_n^z = 0\,, \tag{114}$$

$$\nabla_0^2 \mathcal{M}_{n,t}^z = \frac{1-\nu}{\pi}\left\{-\frac{(\mathbf{n}\cdot\mathbf{X})}{r^4}+4\frac{(\mathbf{n}\cdot\mathbf{X})(\mathbf{t}\cdot\mathbf{X})^2}{r^6}+\left[\frac{(\mathbf{n}\cdot\mathbf{X})^2-(\mathbf{t}\cdot\mathbf{X})^2}{r^4}\right]\alpha_{,t}\right\}, \tag{115}$$

$$\nabla_0^2 \bar{V}_n^z = -\nabla_0^2 \mathcal{M}_{n,t}^z\,. \tag{116}$$

Finally, differentiation of eqns. (111) through (116) gives the gradients of the Laplacian

$$\nabla_0^2 u_{:i}^z = -\frac{6(1-\nu^2)}{\pi E h^3}\frac{X_i}{r^2}\,, \tag{117}$$

$$\nabla_0^2 \phi_{t:i}^z = \frac{6(1-\nu^2)}{\pi E h^3}\left[\frac{n_i}{r^2}-2(\mathbf{n}\cdot\mathbf{X})\frac{X_i}{r^4}\right], \tag{118}$$

$$\nabla_0^2 \mathcal{M}_{t:i}^z = -\frac{2(1-\nu)}{\pi}\left[\frac{X_i+(\mathbf{n}\cdot\mathbf{X})n_i}{r^4}-2(\mathbf{n}\cdot\mathbf{X})^2\frac{X_i}{r^6}\right], \tag{119}$$

$$\nabla_0^2 V_{n:i}^z = 0\,, \tag{120}$$

$$\nabla_0^2 \mathcal{M}_{n,t:i}^z = \frac{1-\nu}{\pi}\left\{\frac{n_i}{r^4}-4\left[\frac{(\mathbf{t}\cdot\mathbf{X})^2 n_i+2(\mathbf{n}\cdot\mathbf{X})(\mathbf{t}\cdot\mathbf{X})t_i+(\mathbf{n}\cdot\mathbf{X})X_i}{r^6}\right]+24(\mathbf{n}\cdot\mathbf{X})(\mathbf{t}\cdot\mathbf{X})^2\frac{X_i}{r^8}\right.$$
$$\left.+2\left[\frac{(\mathbf{t}\cdot\mathbf{X})t_i-(\mathbf{n}\cdot\mathbf{X})n_i}{r^4}+2\{(\mathbf{n}\cdot\mathbf{X})^2-(\mathbf{t}\cdot\mathbf{X})^2\}\frac{X_i}{r^6}\right]\alpha_{,t}\right\}, \tag{121}$$

$$\nabla_0^2 \bar{V}_{n:i}^z = -\nabla_0^2 \mathcal{M}_{n,t:i}^z\,. \tag{122}$$

12. Governing Equations on the Plate Boundary in the Curvilinear *nt*–system

Once the values of u, ϕ_t, $\mathcal{M}_t$ and $\bar{V}_n$ are known on the boundary, the various tensorial quantities of plate theory may be determined on the boundary in the boundary nt–system. The base vectors of the

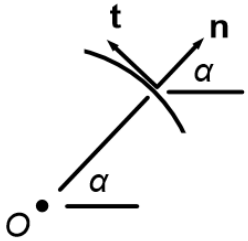

Figure 6. A segment of plate boundary possessing positive curvature.

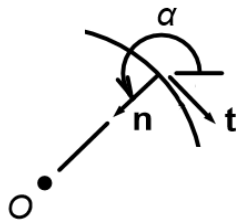

Figure 7. A segment of plate boundary possessing negative curvature.

system are given in terms of angle α by eqns. (50) of **§6**. Figures 6 and 7 directly above show, respectively, portions of the boundary with positive and negative curvatures. The point O in the figures is the instantaneous center of curvature. The curvature c is

$$c \equiv \frac{1}{n} = \alpha_{,t}\,, \qquad \mathrm{d}t = n\mathrm{d}\alpha \;\text{ or }\; \mathrm{d}\alpha = c\mathrm{d}t\,. \tag{123}$$

Note that the n–coordinate is like the r–coordinate of polar coordinates, and that the α–coordinate is like the θ–coordinate of polar coordinates. Consistent with eqns. (50), the derivatives of the base vectors are

$$\mathbf{n}_{,\alpha} = \mathbf{t}\,, \qquad \mathbf{t}_{,\alpha} = -\mathbf{n}\,, \tag{124}$$

and the gradient operator is

$$\boldsymbol{\nabla} = \mathbf{n}\frac{\partial}{\partial n} + \mathbf{t}\frac{\partial}{\partial t} = \mathbf{n}\frac{\partial}{\partial n} + \mathbf{t}\frac{1}{n}\frac{\partial}{\partial \alpha} = \mathbf{n}\frac{\partial}{\partial n} + \mathbf{t}\,c\frac{\partial}{\partial \alpha}\,. \tag{125}$$

Thus, $\boldsymbol{\nabla} u = u_{,n}\mathbf{n} + u_{,t}\mathbf{t}$ so that the rotations are

$$\phi_n = u_{,t}\,, \qquad \phi_t = -u_{,n}\,. \tag{126}$$

The curvatures are $\boldsymbol{\kappa} = \boldsymbol{\nabla}\boldsymbol{\nabla} u$, or

$$\kappa_{nn} = u_{,nn}\,, \qquad \kappa_{tt} = u_{,tt} + cu_{,n}\,, \qquad \kappa_{nt} = \kappa_{tn} = u_{,nt} - cu_{,t}\,, \tag{127}$$

and the moment components then follow Hooke's Law, *i.e.,*

$$\mathcal{M}_n = M_{nn} = -M_{tt} = \frac{Eh^3}{12(1+\nu)}\,\kappa_{nt}\,, \qquad \mathcal{M}_t = M_{nt} = -\frac{Eh^3}{12(1-\nu^2)}\,(\,\kappa_{nn} + \nu\kappa_{tt}\,)\,,$$

$$M_{tn} = \frac{Eh^3}{12(1-\nu^2)}\,(\,\nu\kappa_{nn} + \kappa_{tt}\,)\,. \tag{128}$$

Next, $\nabla^2 u = \boldsymbol{\nabla}\cdot\boldsymbol{\nabla} u = u_{,nn} + u_{,tt} + cu_{,n}$. From this, one finds

$$\boldsymbol{\nabla}\,\nabla^2 u = \left(\,u_{,nnn} + u_{,ntt} + cu_{,nn} - 2cu_{,tt} - c^2 u_{,n}\,\right)\mathbf{n} + \left(\,u_{,nnt} + u_{,ttt} + cu_{,nt}\,\right)\mathbf{t}\,. \tag{129}$$

Consequently, the shear vector is

$$\mathbf{V} = -\frac{Eh^3}{12(1-\nu^2)}\,\boldsymbol{\nabla}\,\nabla^2 u\,, \tag{130}$$

or

$$V_n = -\frac{Eh^3}{12(1-\nu^2)}\left(\,u_{,nnn} + u_{,ntt} + cu_{,nn} - 2cu_{,tt} - c^2 u_{,n}\,\right),$$

$$V_t = -\frac{Eh^3}{12(1-\nu^2)}\left(\,u_{,nnt} + u_{,ttt} + cu_{,nt}\,\right). \tag{131}$$

Finally, the Kirchhoff shear force is $\bar{V}_n = V_n - \mathcal{M}_{n,t}$, which is not a tensorial quantity, and so $\mathcal{M}_{n,t}$ may be calculated just by taking the derivative of $\mathcal{M}_n$ with respect to t. Specifically, putting the curvature κ_{nt} of eqn. (127) into the first of eqns. (128), differentiating, and then using the first of eqns. (131), one obtains

$$\bar{V}_n = -\frac{Eh^3}{12(1-\nu^2)}\left[\,u_{,nnn} + (2-\nu)u_{,ntt} + cu_{,nn} - (3-\nu)cu_{,tt} - c^2 u_{,n} - (1-\nu)c_{,t}u_{,t}\,\right]. \tag{132}$$

We will return to these results, in the context of the numerical method, later in **§17**.

Notwithstanding, once any tensorial quantities are known on the boundary, they may be transformed to the Cartesian xy–system as follows. Let

$$\psi_{ij} = \begin{bmatrix} \cos\alpha & \sin\alpha \\ -\sin\alpha & \cos\alpha \end{bmatrix}. \tag{133}$$

Then, with obvious notation,

$$\phi_j^{xy} = \phi_i^{nt}\psi_{ij}\,, \qquad M_{kl}^{xy} = M_{ij}^{nt}\psi_{ik}\psi_{jl}\,, \qquad V_j^{xy} = V_i^{nt}\psi_{ij}\,. \tag{134}$$

13. Example − Bubble Distributed Load on a Rectangular Plate

At this point, all the theoretical developments needed to implement the Boundary Element Method have been presented. Here, the solution is to a simple problem in Cartesian coordinates is presented, which problem will be solved numerically later in **§20**.

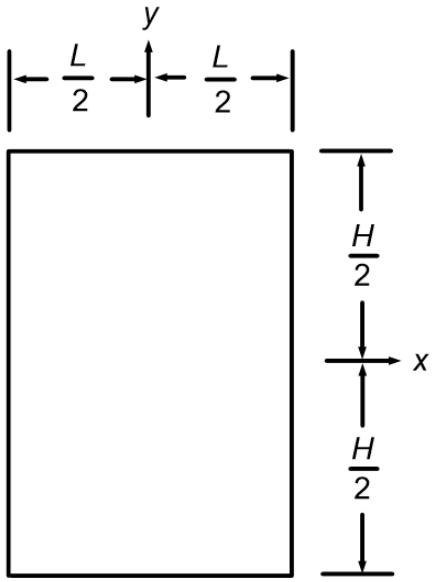

Figure 8. Domain of an L by H rectangular plate.

The domain of the rectangular plate under consideration is shown at left in Fig. 8. The plate is subject to the distributed load

$$q = -\frac{\pi^2 F}{4LH}\cos\left(\frac{\pi x}{L}\right)\cos\left(\frac{\pi y}{H}\right), \tag{135}$$

where $F > 0$ is the net downward force of the distribution, *i.e.,*

$$\int_A q\mathrm{d}A = -F\,. \tag{136}$$

Note that q is zero on the boundary and is maximum at the origin. Hence the term "bubble." On all four faces the boundary conditions are

$$u = 0\,, \qquad \mathcal{M}_t = 0\,, \tag{137}$$

which are the so-called "simply-supported" boundary conditions.

The governing eqn. (9) in **§1** is, via eqn. (135),

$$u_{,xxxx} + 2u_{,xxyy} + u_{,yyyy} = -\frac{3\pi^2(1-\nu^2)F}{Eh^3LH}\cos\left(\frac{\pi x}{L}\right)\cos\left(\frac{\pi y}{H}\right), \tag{138}$$

which is solved with a displacement of the form

$$u = k\cos\left(\frac{\pi x}{L}\right)\cos\left(\frac{\pi y}{H}\right). \tag{139}$$

Substituting eqn. (139) into eqn. (138) gives that

$$k = -\frac{3(1-\nu^2)}{\pi^2 Eh^3}\left[\frac{L^3H^3}{(L^2+H^2)^2}\right]F. \tag{140}$$

With eqns. (139) and (140) the problem is solved.

By differentiation of eqn. (139) by way of eqns. (2) of **§1**, the rotation vector is

$$\phi_x = \frac{3(1-\nu^2)}{\pi^2 Eh^3}\left[\frac{L^3H^2}{(L^2+H^2)^2}\right]F\cos\left(\frac{\pi x}{L}\right)\sin\left(\frac{\pi y}{H}\right),$$

$$\phi_y = -\frac{3(1-\nu^2)}{\pi^2 Eh^3}\left[\frac{L^2H^3}{(L^2+H^2)^2}\right]F\sin\left(\frac{\pi x}{L}\right)\cos\left(\frac{\pi y}{H}\right). \tag{141}$$

Now, using eqns. (2) and (3) of **§1**, the moment components are

$$M_{xx} = -M_{yy} = -\frac{(1-\nu)F}{4}\left[\frac{L^2H^2}{(L^2+H^2)^2}\right]\sin\left(\frac{\pi x}{L}\right)\sin\left(\frac{\pi y}{H}\right),$$

$$M_{xy} = -\frac{F}{4}\left[\frac{LH(\nu L^2+H^2)}{(L^2+H^2)^2}\right]\cos\left(\frac{\pi x}{L}\right)\cos\left(\frac{\pi y}{H}\right), \tag{142}$$

$$M_{yx} = \frac{F}{4}\left[\frac{LH(L^2+\nu H^2)}{(L^2+H^2)^2}\right]\cos\left(\frac{\pi x}{L}\right)\cos\left(\frac{\pi y}{H}\right).$$

Finally, differentiating eqns. (142) via eqns. (5) of **§1**, one obtains the components of the shear vector

$$V_x = \frac{\pi F}{4}\left[\frac{H}{L^2+H^2}\right]\sin\left(\frac{\pi x}{L}\right)\cos\left(\frac{\pi y}{H}\right), \qquad V_y = \frac{\pi F}{4}\left[\frac{L}{L^2+H^2}\right]\cos\left(\frac{\pi x}{L}\right)\sin\left(\frac{\pi y}{H}\right). \tag{143}$$

Note that both the displacement u and the bending moments M_{xy} and M_{yx} are zero on the boundary so that the boundary conditions (137) are satisfied.

On the right $(x = L/2)$ and top $(y = H/2)$ boundaries, respectively, the Kirchhoff shear force is

$$\bar{V}_n^{\text{right}} = V_x - M_{xx,y} = \frac{\pi HF}{4}\left[\frac{(2-\nu)L^2+H^2}{(L^2+H^2)^2}\right]\cos\left(\frac{\pi y}{H}\right),$$

$$\bar{V}_n^{\text{top}} = V_y + M_{yy,x} = \frac{\pi LF}{4}\left[\frac{L^2+(2-\nu)H^2}{(L^2+H^2)^2}\right]\cos\left(\frac{\pi x}{L}\right). \tag{144}$$

At the upper right corner, the normal moment vector $\mathcal{M}_n^- = M_{xx}$ before the corner and $\mathcal{M}_n^+ = M_{yy}$ after the corner are

$$\mathcal{M}_n^- = -\mathcal{M}_n^+ = -\frac{(1-\nu)F}{4}\left[\frac{L^2H^2}{(L^2+H^2)^2}\right] \tag{145}$$

so that the corner force (at the upper right corner) is

$$\mathcal{M}_n^- - \mathcal{M}_n^+ = -\frac{(1-\nu)F}{2}\left[\frac{L^2H^2}{(L^2+H^2)^2}\right]. \tag{146}$$

14. Example – Sinusoidal Transverse Edge Load on an Annular Cantilever Plate

Here a problem in polar coordinates is solved, which problem later will be solved numerically in **§21**. Specifically, below in Fig. 9 is shown the domain of a quarter-annular plate. The distributed load q is zero. The boundaries at $\theta = 0$ and $\theta = \pi/2$ are simply supported, *i.e.*,

$$u = 0\,, \qquad \mathcal{M}_t = 0\,, \tag{147}$$

while the inner radius $r = a$ is built in, *i.e.*,

$$u = \phi_t = 0\,. \tag{148}$$

A transverse sinusoidal edge traction is applied to the outer radius $r = b$, *viz.,*

$$\mathcal{M}_t = 0\,, \qquad \bar{V}_n = \frac{2F}{b}\sin 4\theta\,, \tag{149}$$

where $F > 0$ is the total force of the traction over the interval $\theta \in [\,0\,,\ \pi/4\,]$.

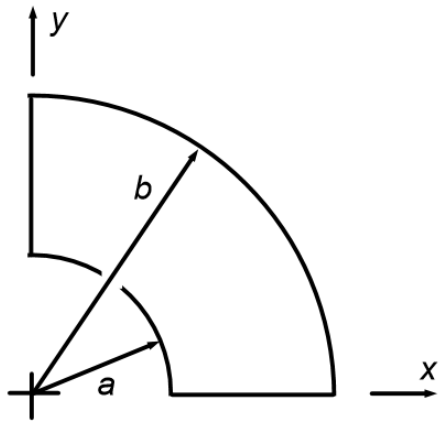

Figure 9. The quarter-annular plate under consideration.

This problem may be solved with a displacement of the form

$$u = f(r)\sin 4\theta \ . \tag{150}$$

With eqn. (150) and eqns. (10) of **§2**, the components of the rotation vector are

$$\phi_r = \frac{4}{r} f \cos 4\theta \ , \qquad \phi_\theta = -f' \sin 4\theta \ . \tag{151}$$

Next, via eqns. (11) and (12) of **§2**, the moments are

$$\begin{aligned} M_{rr} &= -M_{\theta\theta} = \frac{Eh^3}{3(1+\nu)} \left(\frac{1}{r} f' - \frac{1}{r^2} f \right) \cos 4\theta, \\ M_{r\theta} &= -\frac{Eh^3}{12(1-\nu^2)} \left(f'' + \frac{\nu}{r} f' - \frac{16\nu}{r^2} f \right) \sin 4\theta \ , \\ M_{\theta r} &= \frac{Eh^3}{12(1-\nu^2)} \left(\nu f'' + \frac{1}{r} f' - \frac{16}{r^2} f \right) \sin 4\theta \ . \end{aligned} \tag{152}$$

Finally, eqns. (14) of **§2** give the components of the shear vector

$$\begin{aligned} V_r &= -\frac{Eh^3}{12(1-\nu^2)} \left(f''' + \frac{1}{r} f'' - \frac{17}{r^2} f' + \frac{32}{r^3} f \right) \sin 4\theta \ , \\ V_\theta &= -\frac{Eh^3}{3(1-\nu^2)} \left(\frac{1}{r} f'' + \frac{1}{r^2} f' - \frac{16}{r^3} f \right) \cos 4\theta \ . \end{aligned} \tag{153}$$

On the boundary, the Kirchhoff shear forces are

$$\begin{aligned} &r = b \ \Rightarrow \ \bar{V}_n = V_r - \frac{1}{r} \frac{\mathrm{d}M_{rr}}{\mathrm{d}\theta} \ , \qquad \theta = 0 \ \Rightarrow \ \bar{V}_n = -V_\theta - \frac{\mathrm{d}M_{\theta\theta}}{\mathrm{d}r} \ , \\ &\theta = \pi/2 \ \Rightarrow \ \bar{V}_n = V_\theta + \frac{\mathrm{d}M_{\theta\theta}}{\mathrm{d}r} \ , \qquad r = a \ \Rightarrow \ \bar{V}_n = -V_r + \frac{1}{r} \frac{\mathrm{d}M_{rr}}{\mathrm{d}\theta} \ , \end{aligned} \tag{154}$$

or, respectively, for $r = b$, $\theta = 0$, $\theta = \pi/2$ and $r = a$,

$$\begin{aligned} \bar{V}_n &= -\frac{Eh^3}{12(1-\nu^2)} \left[f''' + \frac{1}{b} f'' - \frac{(33-16\nu)}{b^2} f' + \frac{16(3-\nu)}{b^3} f \right] \sin 4\theta \ , \\ \bar{V}_n &= \frac{Eh^3}{12(1-\nu^2)} \left[\frac{4(2-\nu)}{r} f'' - \frac{4(1-2\nu)}{r^2} f' - \frac{8(7+\nu)}{r^3} f \right] , \\ \bar{V}_n &= -\frac{Eh^3}{12(1-\nu^2)} \left[\frac{4(2-\nu)}{r} f'' - \frac{4(1-2\nu)}{r^2} f' - \frac{8(7+\nu)}{r^3} f \right] , \\ \bar{V}_n &= \frac{Eh^3}{12(1-\nu^2)} \left[f''' + \frac{1}{a} f'' - \frac{(33-16\nu)}{a^2} f' + \frac{16(3-\nu)}{a^3} f \right] \sin 4\theta \ . \end{aligned} \tag{155}$$

Now, substituting the displacement (150) into the governing equation $\nabla^4 u = 0$, *cf.*, eqn. (15) in **§2**, one obtains the differential equation

$$f'''' + \frac{2}{r} f''' - \frac{33}{r^2} f'' + \frac{33}{r^3} f' + \frac{192}{r^4} f = 0 \, . \tag{156}$$

The solution to eqn. (156) is

$$f = \frac{k_1}{r^4} + \frac{k_2}{r^2} + k_3 r^4 + k_4 r^6 \,,$$

$$f' = -4\frac{k_1}{r^5} - 2\frac{k_2}{r^3} + 4k_3 r^3 + 6k_4 r^5 \,,$$

$$f'' = 20\frac{k_1}{r^6} + 6\frac{k_2}{r^4} + 12k_3 r^2 + 30k_4 r^4 \,, \tag{157}$$

$$f''' = -120\frac{k_1}{r^7} - 24\frac{k_2}{r^5} + 24k_3 r + 120k_4 r^3 \,.$$

Looking at eqns. (150) and (152), one sees that the boundary conditions (147) are satisfied identically. The conditions, respectively, $u(a,\theta) = 0$, $\phi_t = -\phi_\theta(a,\theta) = 0$, $\mathcal{M}_t = M_{r\theta}(b,\theta) = 0$ and $\bar{V}_n = (2F/b)\sin 4\theta$ yield the system of equations to satisfy the boundary conditions (148) and (149), *viz.*,

$$\begin{bmatrix} 1/a^4 & 1/a^2 & a^4 & a^6 \\ -2/a^5 & -1/a^3 & 2a^3 & 3a^5 \\ 10(1-\nu)/b^6 & 3(1-3\nu)/b^4 & 6(1-\nu)b^2 & 5(3-\nu)b^4 \\ -5(1-\nu)/b^6 & -3(2-\nu)/b^4 & 3(1-\nu)b^2 & -5\nu b^4 \end{bmatrix} \begin{bmatrix} k_1 \\ k_2 \\ k_3 \\ k_4 \end{bmatrix} = \begin{bmatrix} 0 \\ 0 \\ 0 \\ 3(1-\nu^2)F/(2Eh^3) \end{bmatrix} . \tag{158}$$

Using the constants

$$E = 3.0 \times 10^7 \text{ psi} \,, \quad \nu = 0.3 \,, \quad h = 1.0 \text{ in} \,, \quad F = 10\,000 \text{ lb} \,, \quad a = 120 \text{ in} \,, \quad b = 360 \text{ in} \,, \tag{159}$$

the solution to eqn. (158) is

$$k_1 = 1.666\,591\,940\,231\,4806 \times 10^8 \,, \qquad k_2 = -1.547\,802\,450\,020\,5023 \times 10^4 \,,$$

$$k_3 = 1.354\,435\,354\,756\,7996 \times 10^{-9} \,, \qquad k_4 = -3.252\,532\,373\,598\,9290 \times 10^{-15} \tag{160}$$

which constants solve the problem at hand.

As a final comment, for the constants (159) and (160), the values of the four corner forces are

Corner Force at (r,θ)	Value (lb)
$(M_{\theta\theta} - M_{rr})(a,0)$	0
$(M_{\theta\theta} - M_{rr})(b,0)$	−3935.94
$(M_{rr} - M_{\theta\theta})(b,\pi/2)$	3935.94
$(M_{rr} - M_{\theta\theta})(a,\pi/2)$	0

15. A 14-degree-of-freedom Curved Boundary Element

Figure 10 below shows the geometry of the boundary element. The length of the element is L, and along the element, the tangential coordinate is $t \in [\,0\,, L\,]$ and the normalized tangential coordinate is $\xi \in [\,-1\,, 1\,]$, *i.e.*,

$$t = \frac{L}{2}(\xi + 1) \,, \qquad \frac{\mathrm{d}\xi}{\mathrm{d}t} = \frac{2}{L} \,. \tag{161}$$

In Fig. 10, α_0 and α_1 are the nodal values of the angle α defined in Fig. 5 of **§6**. The element may be either straight or curved, and if it is curved, it is a circular arc. The node 2 is located at $\xi = 0$. Notwithstanding, the linear interpolation functions are

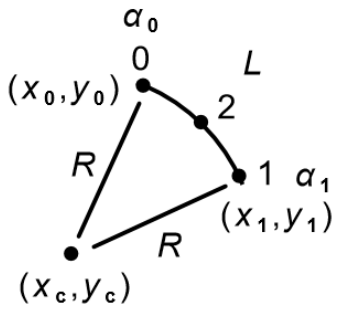

Figure 10. Geometry of the boundary element as described in the text.

$$d^0 = \frac{1}{2}(1-\xi)\,, \qquad d^1 = \frac{1}{2}(1+\xi)\,. \tag{162}$$

If $\alpha_0 = \alpha_1$, then the element is straight, and the xy–coordinates are interpolated as

$$x_i = d^I x_{Ii}\,, \tag{163}$$

and in this case, the length of the element is

$$L = \sqrt{(x_1 - x_0)^2 + (y_1 - y_0)^2}\,. \tag{164}$$

If the element is curved, it has $(x_c\,, y_c)$ as the center of curvature, and the radius of curvature R is constant, as is the curvature $c = 1/R$. Here the angle α is interpolated through the element as

$$\alpha = d^I \alpha_I\,, \tag{165}$$

and the curvature and element length are given by

$$c = \frac{\cos\alpha_1 - \cos\alpha_0}{x_1 - x_0} \;\text{ or }\; c = \frac{\sin\alpha_1 - \sin\alpha_0}{y_1 - y_0} \quad \Rightarrow \quad L = \frac{\alpha_1 - \alpha_0}{c}\,. \tag{166}$$

For the curved element, the xy–coordinates are interpolated along the element via

$$x = \frac{\cos\alpha}{c}\,, \qquad y = \frac{\sin\alpha}{c}\,. \tag{167}$$

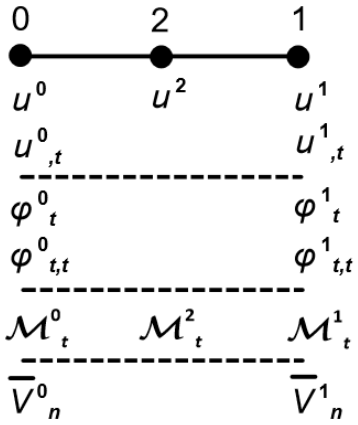

Figure 11. Degrees-of-freedom of the boundary element.

The degrees-of-freedom of the boundary element are shown at left in Fig. 11. The displacement u is interpolated through the element as a quartic; the tangential rotation ϕ_t, a cubic; the tangential bending moment $\mathcal{M}_t$, a quadratic; and finally, the Kirchhoff shear force $\bar{V}_n$, as a linear function. The decreasing orders of these interpolations are consistent with the governing equations of plate theory.

The Kirchhoff shear force is interpolated through the element via

$$\bar{V}_n = d^0 \bar{V}_n^0 + d^1 \bar{V}_n^1\,, \tag{168}$$

where the functions d^I are given above in eqns. (162).

The tangential bending moment is interpolated as

$$\mathcal{M}_t = c^0 \mathcal{M}_t^0 + c^1 \mathcal{M}_t^2 + c^2 \mathcal{M}_t^1\,, \tag{169}$$

where

$$c^0 = \frac{1}{2}(-\xi + \xi^2)\,, \qquad c^1 = 1 - \xi^2\,, \qquad c^2 = \frac{1}{2}(\xi + \xi^2)\,. \tag{170}$$

If $\mathcal{M}_{t,t}$ is needed in the element, then eqns. (170) may be differentiated via

$$\frac{\mathrm{d}c^I}{\mathrm{d}t} = \frac{\mathrm{d}c^I}{\mathrm{d}\xi}\,\frac{\mathrm{d}\xi}{\mathrm{d}t} = \frac{2}{L}\,\frac{\mathrm{d}c^I}{\mathrm{d}\xi}\,. \tag{171}$$

The tangential rotation is interpolated with

$$\phi_t = b^0\phi_t^0 + b^1\phi_{t,t}^0 + b^2\phi_t^1 + b^3\phi_{t,t}^1 \,, \tag{172}$$

where

$$b^0 = \frac{1}{4}(2 - 3\xi + \xi^3) \,, \qquad b^1 = \frac{L}{8}(1 - \xi - \xi^2 + \xi^3) \,,$$
$$b^2 = \frac{1}{4}(2 + 3\xi - \xi^3) \,, \qquad b^3 = \frac{L}{8}(-1 - \xi + \xi^2 + \xi^3) \,. \tag{173}$$

As before, if one requires the derivatives of ϕ_t within the element, the technique of eqn. (171) may be employed.

Finally, in the element, the displacement u follows

$$u = a^0u^0 + a^1u_{,t}^0 + a^2u^2 + a^3u^1 + a^4u_{,t}^1 \,, \tag{174}$$

where

$$a^0 = \frac{1}{4}(-3\xi + 4\xi^2 + \xi^3 - 2\xi^4) \,, \qquad a^1 = \frac{L}{8}(-\xi + \xi^2 + \xi^3 - \xi^4) \,, \qquad a^2 = 1 - 2\xi^2 + \xi^4 \,,$$
$$a^3 = \frac{1}{4}(3\xi + 4\xi^2 - \xi^3 - 2\xi^4) \,, \qquad a^4 = \frac{L}{8}(-\xi - \xi^2 + \xi^3 + \xi^4) \,. \tag{175}$$

Once again, if the derivatives of u are needed in the element, they can be calculated by using the chain rule, as in eqn. (171).

Now, define the element nodal vector v^I by

$$v^I = \begin{bmatrix} v^0 \\ v^1 \\ v^2 \\ v^3 \\ v^4 \\ v^5 \end{bmatrix} = \begin{bmatrix} u^0 \\ u_{,t}^0 \\ \phi_t^0 \\ \phi_{t,t}^0 \\ \mathcal{M}_t^0 \\ \bar{V}_n^0 \end{bmatrix}, \quad A^I = \begin{bmatrix} a^0 \\ a^1 \\ 0 \\ 0 \\ 0 \\ 0 \end{bmatrix}, \quad B^I = \begin{bmatrix} 0 \\ 0 \\ b^0 \\ b^1 \\ 0 \\ 0 \end{bmatrix}, \quad C^I = \begin{bmatrix} 0 \\ 0 \\ 0 \\ 0 \\ c^0 \\ 0 \end{bmatrix}, \quad D^I = \begin{bmatrix} 0 \\ 0 \\ 0 \\ 0 \\ 0 \\ d^0 \end{bmatrix},$$
$$\begin{bmatrix} v^6 \\ v^7 \\ v^8 \\ v^9 \\ v^{10} \\ v^{11} \\ v^{12} \\ v^{13} \end{bmatrix} = \begin{bmatrix} u^2 \\ \mathcal{M}_t^2 \\ u^1 \\ u_{,t}^1 \\ \phi_t^1 \\ \phi_{t,t}^1 \\ \mathcal{M}_t^1 \\ \bar{V}_n^1 \end{bmatrix}, \quad \begin{bmatrix} a^2 \\ 0 \\ a^3 \\ a^4 \\ 0 \\ 0 \\ 0 \\ 0 \end{bmatrix}, \quad \begin{bmatrix} 0 \\ 0 \\ b^2 \\ b^3 \\ 0 \\ 0 \end{bmatrix}, \quad \begin{bmatrix} 0 \\ c^1 \\ 0 \\ 0 \\ 0 \\ 0 \\ c^2 \\ 0 \end{bmatrix}, \quad \begin{bmatrix} 0 \\ 0 \\ 0 \\ 0 \\ 0 \\ 0 \\ 0 \\ d^1 \end{bmatrix}, \tag{176}$$

which allows the interpolations (168), (169), (172) and (174) to be written more compactly as

$$u = A^I v^I \,, \qquad \phi_t = B^I v^I \,, \qquad \mathcal{M}_t = C^I v^I \,, \qquad \bar{V}_n = D^I v^I \,. \tag{177}$$

16. Boundary Solution via the Boundary Element Method

The Reciprocal Theorem, *i.e.,* eqn. (80) in **§8**, or eqn. (92) in **§9** with the singularity point $\mathbf{x}^0$ outside of the plate domain A ($\beta = 0$), restated is

$$\oint_t u\bar{V}_n^k \mathrm{d}t + \oint_t \phi_t \mathcal{M}_t^k \mathrm{d}t - \oint_t \mathcal{M}_t \phi_t^k \mathrm{d}t - \oint_t \bar{V}_n u^k \mathrm{d}t = \int_A u^k q \mathrm{d}A \,, \tag{178}$$

where here, $k \equiv x$ and $k \equiv y$ refer to the MGFs, and $k \equiv z$ refers to the TGF. Substituting the interpolations (177) into (178), one obtains the discretized form

$$K^{kI} v^I = L^k \,, \tag{179}$$

where

$$K^{kI} = \int_t \left(A^I \bar{V}_n^k + B^I \mathcal{M}_t^k - C^I \phi_t^k - D^I u^k \right) \mathrm{d}t \,, \qquad L^k = \int_A q u^k \mathrm{d}A \,, \tag{180}$$

which equations may be integrated around the boundary circuit, and over the domain A if $q \neq 0$.

Generating an equation for each unknown boundary value depends on the boundary conditions, of which there are four common cases as listed in the table.

Case	Prescribed Values	Unknown Values
1	u , ϕ_t	$\mathcal{M}_t$, $\bar{V}_n$
2	u , $\mathcal{M}_t$	ϕ_t , $\bar{V}_n$
3	ϕ_t , $\bar{V}_n$	u , $\mathcal{M}_t$
4	$\mathcal{M}_t$, $\bar{V}_n$	u , ϕ_t

Figure 12 below shows a schematic of the boundary element for the boundary condition case 1. The red quantities are prescribed, so no equations need to be generated for them. On the other hand, the black quantities are unknown, so that equations need to be generated. For example, node 0 possess two

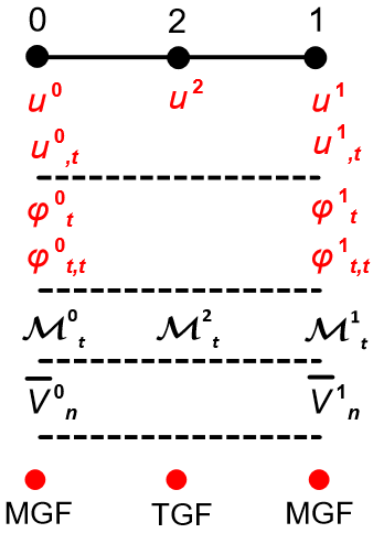

Figure 12. The boundary element for boundary condition case 1.

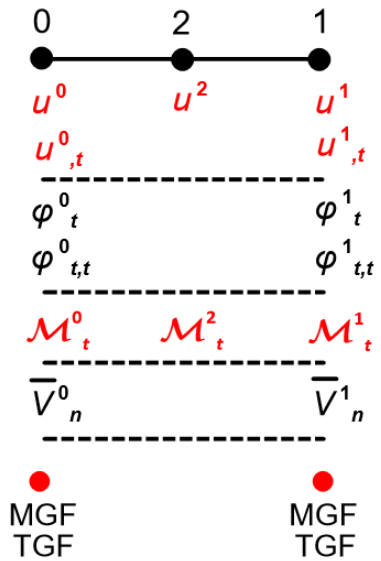

Figure 13. The boundary element for boundary condition case 2.

unknowns, and two equations are obtained by placing the singularity point $\mathbf{x}^0$ outside of the domain A near node 0, as denoted by the red point in the figure, and then two equations are obtained from the two components of the MGFs. Similarly, node 2 possesses one unknown, and placing $\mathbf{x}^0$ outside of A near node 2 and using the TGF generates one equation.

As for boundary condition case 2, depicted above in Fig. 13, node 0 possesses three unknowns. Similarly to case 1, $\mathbf{x}^0$ is placed outside of A near node 0, and using the two components of the MGFs, and the one component of the TGF, yields the needed three equations. Note that for case 2, no equations need to be generated for node 2.

Figure 14 below depicts the boundary condition case 3. The three equations required for node 0 are constructed exactly as they were for node 0 of case 2. For node 2, the two required equations are provided by placing $\mathbf{x}^0$ outside of A near node 2, and by using the two components of the MGFs.

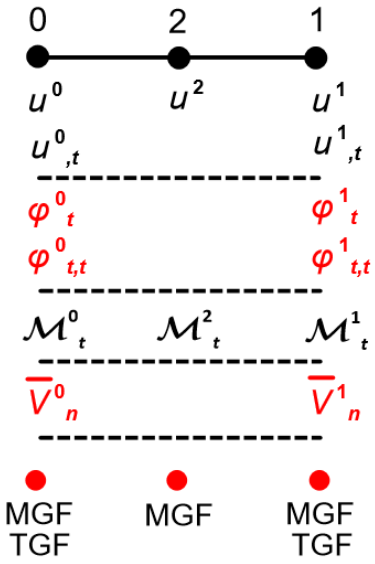

Figure 14. The boundary element for boundary condition case 3.

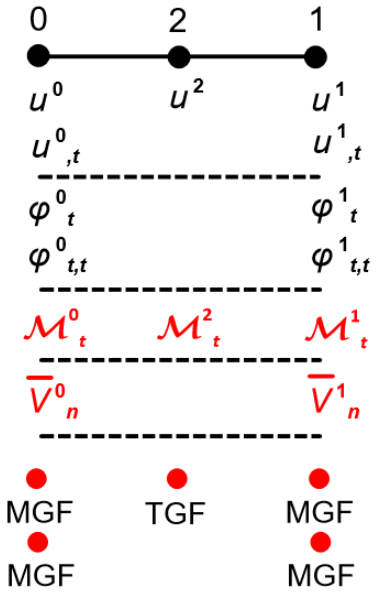

Figure 15. The boundary element for boundary condition case 4.

Boundary condition case 4 is shown by Fig. 15 at above right. Here node 0 possesses four unknowns, and the four equations are obtained by placing two singularity points outside of A near node 0, and then by using the two components of the MGFs at each of the two points. The single equation for node 2 is constructed exactly as was done for node 2 of boundary condition case 1.

Turning attention to the integration of the second of eqns. (180), the interior A of the domain is discretized with a grid of bi-linear integrations cells. Each integration cell, in fact, is just the usual bi-linear iso-parametric finite element. Figure 16 below shows the cell in normalized $\boldsymbol{\xi}$–space, whose differential of area is $\mathrm{d}A^*$, and Fig.17 shows the cell in physical space, whose differential of area is $\mathrm{d}A$. With the linear functions

$$f^0 = \frac{1}{2}(1-\xi)\,, \qquad f^1 = \frac{1}{2}(1+\xi)\,, \tag{181}$$

the interpolation functions of the cell are

$$S^0 = f^0(\xi_0)f^0(\xi_1)\,, \quad S^1 = f^1(\xi_0)f^0(\xi_1)\,, \quad S^2 = f^0(\xi_0)f^1(\xi_1)\,, \quad S^3 = f^1(\xi_0)f^1(\xi_1)\,. \tag{182}$$

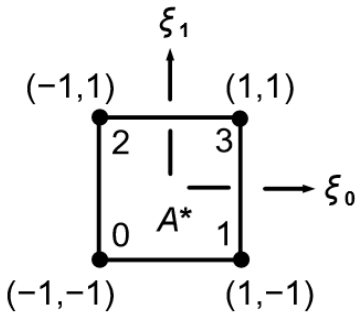

Figure 16. Integration cell in normalized $\boldsymbol{\xi}$–space.

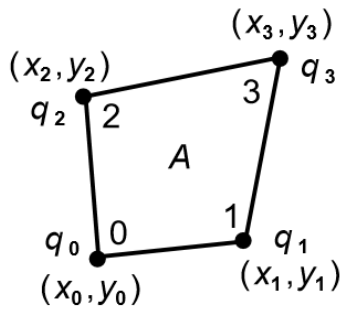

Figure 17. Integration cell in physical space.

The geometry and distributed load are then represented in the interior of the cell via

$$x_i = S^I x_{Ii}\,, \qquad q = S^I q_I\,. \tag{183}$$

Now,

$$\mathrm{d}x_i = \frac{\partial x_i}{\partial \xi_\alpha}\,\mathrm{d}\xi_\alpha\,, \qquad \frac{\partial x_i}{\partial \xi_\alpha} = S^I_{,\alpha} x_{Ii} \equiv A_{i\alpha}\,, \qquad \mathrm{d}x_i = A_{i\alpha}\mathrm{d}\xi_\alpha \;\Rightarrow\; \mathrm{d}A = (\det \mathbf{A})\mathrm{d}A^*\,. \tag{184}$$

Thus, the integral

$$\int_A \mathcal{F}\mathrm{d}A = \int_{A^*} \mathcal{F}(\det \mathbf{A})\mathrm{d}A^* = \int_{-1}^{1}\int_{-1}^{1} \mathcal{F}(\det \mathbf{A})\mathrm{d}\xi_0\mathrm{d}\xi_1 \approx \sum_{n=1}^{\mathrm{O}}\sum_{m=1}^{\mathrm{O}} (\mathcal{F}\det \mathbf{A})(\xi_0^n, \xi_1^m) w_n w_m\,, \tag{185}$$

where ξ^n and w_n are, respectively, the points and weights of a Gauss-Legendre quadrature rule of order O.

The integration of the first of eqns. (180) is also performed with Gauss-Legendre quadrature, *viz.,*

$$\int_t \mathcal{F}dt = \int_0^L \mathcal{F}\mathrm{d}t = \frac{L}{2}\int_{-1}^{1} \mathcal{F}d\xi \approx \frac{L}{2}\sum_{n=1}^{\mathrm{O}} \mathcal{F}(\xi^n) w_n\,. \tag{186}$$

Finally, the corner forces occurring in eqn. (178) need to be accounted for. When integrating around a corner, as depicted at left in Fig. 18, the Green's functions possess corner forces. Namely, to the left-hand side of the first of eqns. (178), one must add

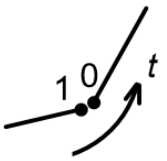

Figure 18. Integrating around a corner formed by two adjoining boundary elements.

$$\left(M_{nn}^k\right)^1 u - \left(M_{nn}^k\right)^0 u\,, \tag{187}$$

where u is the displacement degree-of-freedom at the corner. The solution itself also possesses corner forces $\mathrm{c.f.}^I$, which are degrees-of-freedom in the system of equations to solve. So, when integrating around a corner, one must also add

$$-u^k \mathrm{c.f.}^I \tag{188}$$

to the left-hand side of the first of eqns. (178). Since the solution corner forces are degrees-of-freedom of the system, for each unknown corner force, a single equation is constructed by putting the singularity point $\mathbf{x}^0$ outside of A near the corner, and by using the single component of the TGF.

Having constructed all the equations for the unknown degrees-of-freedom, enforcing the values of the know degrees-of-freedom yields a linear system to solve for the boundary values of u, ϕ_t, $\mathcal{M}_t$

and $\bar{V}_n$.

17. Calculation of Boundary Tensorial Quantities from the Boundary Solution

Once the boundary values of u, ϕ_t, $\mathcal{M}_t$ and $\bar{V}_n$ are known, finding all the plate tensorial values on the boundary in nt–system can be done as follows.

From eqns. (127) and (128) of **§12**,

$$\mathcal{M}_t = -\frac{Eh^3}{12(1-\nu^2)}\left(u_{,nn} + \nu u_{,tt} + \nu c u_{,n} \right) \quad \Rightarrow \quad u_{,nn} = -\nu u_{,tt} - \nu c u_{,n} - \frac{12(1-\nu^2)}{Eh^3}\mathcal{M}_t \,. \tag{189}$$

Substituting the interpolations of **§15**, *i.e.,* $u_{,tt} = A^I_{,tt} v^I$, $\phi_t = -u_{,n} = B^I v^I$ and $\mathcal{M}_t = C^I v^I$ into eqn. (189) yields

$$u_{,nn} = F^I v^I \,, \qquad F^I = -\nu A^I_{,tt} + \nu c B^I - \frac{12(1-\nu^2)}{Eh^3} C^I \,, \tag{190}$$

and

$$u_{,nnt} = F^I_{,t} v^I \,, \qquad F^I_{,t} = -\nu A^I_{,ttt} + \nu c B^I_{,t} - \frac{12(1-\nu^2)}{Eh^3} C^I_{,t} \,, \tag{191}$$

where v^I is the vector of degrees-of-freedom given by eqn. (176) of **§15**. Next, from eqn. (132) of **§12**,

$$\bar{V}_n = -\frac{Eh^3}{12(1-\nu^2)}\left[u_{,nnn} + (2-\nu) u_{,ntt} + c u_{,nn} - (3-\nu) c u_{,tt} - c^2 u_{,n} \right]. \tag{192}$$

Note that $c_{,t} = 0$ was used in writing down eqn. (192), *i.e.,* the boundary element in **§15** has constant curvature. So, solving eqn. (192) for $u_{,nnn}$ gives

$$u_{,nnn} = (3-\nu) c u_{,tt} + c^2 u_{,n} - (2-\nu) u_{,ntt} - c u_{,nn} - \frac{12(1-\nu^2)}{Eh^3}\bar{V}_n \,. \tag{193}$$

Now, putting $\phi_{t,tt} = -u_{,ntt} = B^I_{,tt} v^I$, eqn. (190) and $\bar{V}_n = D^I v^I$ into (193), one obtains

$$u_{,nnn} = G^I v^I \,, \qquad G^I = (3-\nu) c A^I_{,tt} - c^2 B^I + (2-\nu) B^I_{,tt} - c F^I - \frac{12(1-\nu^2)}{Eh^3} D^I \,. \tag{194}$$

Turning attention to the tensors **M** and **V**, into the expressions for the moments, *i.e.,* eqns. (127) and (128) of **§12**, substitute the interpolations from **§15** and eqn. (190) to obtain the interpolations for the moment components

$$\begin{aligned} &M_{nn} = -M_{tt} = M^I v^I \,, \qquad M^I = -\frac{Eh^3}{12(1+\nu)}\left(B^I_{,t} + c A^I_{,t} \right) \,, \\ &M_{nt} = C^I v^I \,, \\ &M_{tn} = N^I v^I, \qquad N^I = \frac{Eh^3}{12(1-\nu^2)}\left(A^I_{,tt} - c B^I + \nu F^I \right). \end{aligned} \tag{195}$$

Finally, putting the interpolations of **§15** and eqns. (190), (191) and (194) into eqns. (131) of **§12**, the components of the shear vector are

$$\begin{aligned} &V_n = P^I v^I \,, \qquad P^I = -\frac{Eh^3}{12(1-\nu^2)}\left(-2c A^I_{,tt} + c^2 B^I - B^I_{,tt} + c F^I + G^I \right), \\ &V_t = Q^I v^I \,, \qquad Q^I = -\frac{Eh^3}{12(1-\nu^2)}\left(A^I_{,ttt} - c B^I_{,t} + F^I \right). \end{aligned} \tag{196}$$

Notwithstanding, once the various tensors are known in the boundary nt–system, they may be transferred to the xy–system via eqns. (133) and (134) of **§12**.

Looking at Fig. 11 of **§15**, at either node 0 or 1 of the element, u, $u_{,t}$, $u_{,n} = -\phi_t$, $u_{,nt} = -\phi_{t,t}$ and $\mathcal{M}_t = M_{nt}$ are known from the nodal degrees-of-freedom, and thus, these quantities are continuous from one element to another. From eqns. (127) and (128) of **§12**, so is $M_{nn} = -M_{tt}$. The remaining tensor components are, most generally, discontinuous from element to element, *i.e.,* M_{tn}, V_n and V_t. So, to calculate these quantities at the six-degree-of-freedom nodes (nodes 0 or 1 in Fig. 11 of **§15**), averaging between adjacent boundary elements is required, which averaging introduces some amount of error. This error will be discussed below in **§19**.

18. Calculation of Interior Tensorial Quantities from the Boundary Solution

Once the boundary values of u, ϕ_t, $\mathcal{M}_t$ and $\bar{V}_n$ are known, and the solution corner forces c.f.^I are known, the solution in the interior of the domain A can be calculated by putting the interpolations (177) of **§15** into eqns. (93) and (95) through (97) of **§10**. Thus,

$$u(\mathbf{x}^0) = L^z - K^{zI}v^I\,, \qquad u_{:i}(\mathbf{x}^0) = L^z_{:i} - K^{zI}_{:i}v^I\,,$$
$$u_{:ij}(\mathbf{x}^0) = L^z_{:ij} - K^{zI}_{:ij}v^I\,, \qquad \nabla_0^2 u_{:i}(\mathbf{x}^0) = \nabla_0^2 L^z_{:i} - \nabla_0^2 K^{zI}_{:i}v^I\,, \tag{197}$$

where

$$L^z = \int_A qu^z \mathrm{d}A\,, \qquad K^{zI} = \int_t (\,A^I\bar{V}_n^z + B^I\mathcal{M}_t^z - C^I\phi_t^z - D^I u^z\,)\mathrm{d}t\,,$$
$$L^z_{:i} = \int_A qu^z_{:i}\mathrm{d}A\,, \qquad K^{zI}_{:i} = \int_t (\,A^I\bar{V}^z_{n:i} + B^I\mathcal{M}^z_{t:i} - C^I\phi^z_{t:i} - D^I u^z_{:i}\,)\mathrm{d}t\,,$$
$$L^z_{:ij} = \int_A qu^z_{:ij}\mathrm{d}A\,, \qquad K^{zI}_{:ij} = \int_t \big(\,A^I\bar{V}^z_{n:ij} + B^I\mathcal{M}^z_{t:ij} - C^I\phi^z_{t:ij} - D^I u^z_{:ij}\,\big)\mathrm{d}t\,,$$
$$\nabla_0^2 L^z_{:i} = \int_A q\nabla_0^2 u^z_{:i}\mathrm{d}A\,, \qquad \nabla_0^2 K^{zI}_{:i} = \int_t (\,A^I\nabla_0^2\bar{V}^z_{n:i} + B^I\nabla_0^2\mathcal{M}^z_{t:i} - C^I\nabla_0^2\phi^z_{t:i} - D^I\nabla_0^2 u^z_{:i}\,)\mathrm{d}t\,. \tag{198}$$

Similarly to what was described earlier by Fig. 18, and eqns. (187) and (188) of **§16**, the terms due to the corner forces of the TGF

$$+(M^z_{nn})^0 u - (M^z_{nn})^1 u\,, \qquad +(M^z_{nn:i})^0 u - (M^z_{nn:i})^1 u\,,$$
$$+\big(M^z_{nn:ij}\big)^0 u - \big(M^z_{nn:ij}\big)^1 u\,, \qquad +(\nabla_0^2 M^z_{nn:i})^0 u - (\nabla_0^2 M^z_{nn:i})^1 u \tag{199}$$

need to be added to the right-hand sides of eqns. (197), and the terms due to the solution corner forces

$$+u^z\,\text{c.f.}^I\,, \qquad +u^z_{:i}\,\text{c.f.}^I\,, \qquad +u^z_{:ij}\,\text{c.f.}^I\,, \qquad +\nabla_0^2 u^z_{:i}\,\text{c.f.}^I \tag{200}$$

also need to be added to the right-hand sides of eqns. (197).

19. Alternate Calculation of the Shear Vector

As it turns out, for the boundary element of **§15**, for most problems, the calculation of the shear vector **V** in the interior of the plate A using the fourth of eqns. (197) and (198) of **§18** is unacceptably inaccurate. Additionally, calculation of the components of **V** on the boundary by employing eqns. (196) of

§17 (via nodal averaging between adjacent elements) is inaccurate for some problems. The sources of these inaccuracies will be discussed later in **§22**.

Consequently, the shear vector needs to be calculated by an alternate method, *viz.,* by numerical

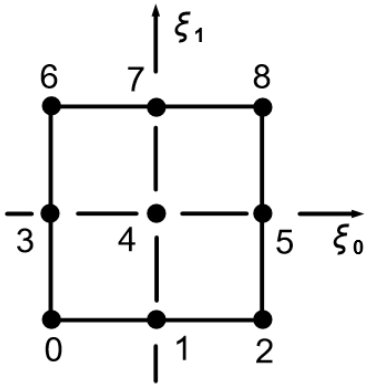

Figure 19. Differentiation cell in normalized **ξ**–space.

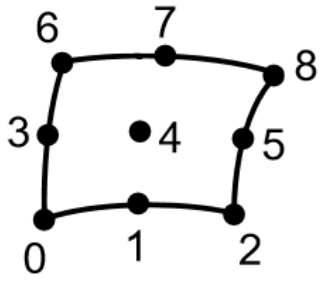

Figure 20. Differentiation cell in physical space.

differentiation of the moment field via

$$V_x = M_{xy,x} + M_{yy,y}\,, \qquad V_y = -M_{xx,x} - M_{yx,y}\,. \tag{201}$$

Figures 19 and 20 show schematics of the differentiation cell, which cell, actually, is just a bi-quadratic iso-parametric finite element. Note that the normalized **ξ**–space is spanned by $\xi_0 \in [\,-1\,,1\,] \times \xi_1 \in [\,-1\,,1\,]$. Notwithstanding, given the quadratics

$$f^0 = \frac{1}{2}\,(-\xi + \xi^2)\,, \qquad f^1 = 1 - \xi^2\,, \qquad f^2 = \frac{1}{2}\,(\xi + \xi^2)\,, \tag{202}$$

the interpolation functions for the cell are

$$\begin{array}{lll} S^0 = f^0(\xi_0)f^0(\xi_1) & S^1 = f^1(\xi_0)f^0(\xi_1) & S^2 = f^2(\xi_0)f^0(\xi_1) \\ S^3 = f^0(\xi_0)f^1(\xi_1) & S^4 = f^1(\xi_0)f^1(\xi_1) & S^5 = f^2(\xi_0)f^1(\xi_1)\,. \\ S^6 = f^0(\xi_0)f^2(\xi_1) & S^7 = f^1(\xi_0)f^2(\xi_1) & S^8 = f^2(\xi_0)f^2(\xi_1) \end{array} \tag{203}$$

The geometry x_i and moment tensor M_{ij} are interpolated within the cell via

$$x_i = S^I x_{Ii}\,, \qquad M_{ij} = S^I M_{Iij}\,, \tag{204}$$

where x_{Ii} are the physical nodal coordinates of the cell, and M_{Iij} are the nodal values of the moment tensor. To calculate the derivatives (201), one sees

$$\mathrm{d}x_i = \frac{\partial x_i}{\partial \xi_\alpha}\mathrm{d}\xi_\alpha \equiv A_{i\alpha}\mathrm{d}\xi_\alpha\,, \qquad A_{i\alpha} = \frac{\partial S^I}{\partial \xi_\alpha}x_{Ii} = S^I_{,\alpha}x_{Ii} \;\Rightarrow\; \mathrm{d}\xi_\alpha = \frac{\partial \xi_\alpha}{\partial x_i}\mathrm{d}x_i\,, \qquad \frac{\partial \xi_\alpha}{\partial x_i} = A^{-1}_{\alpha i}\,. \tag{205}$$

Thus, the physical derivatives of the interpolations are

$$\frac{\partial S^I}{\partial x_i} = S^I_{,i} = \frac{\partial S^I}{\partial \xi_\alpha}\,\frac{\partial \xi_\alpha}{\partial x_i} = S^I_{,\alpha}A^{-1}_{\alpha i} \tag{206}$$

so that the derivatives of the moments are

$$M_{ij,k} = S^I_{,k}M_{Iij}\,. \tag{207}$$

Finally then, via eqns. (207), the derivatives (201) are calculated numerically as

$$V_x = S^I_{,x} M_{Ixy} + S^I_{,y} M_{Iyy} \,, \qquad V_y = -S^I_{,x} M_{Ixx} - S^I_{,y} M_{Iyx} \,. \tag{208}$$

If a computational node is on a corner of the boundary, then eqns. (208) are evaluated at either nodes 0, 2, 6 or 8 of the cell. If the node is on a smooth portion of the boundary, then the derivatives are evaluated at either nodes 1, 3, 5 or 7 of the cell. The derivatives of points internal to A are evaluated at point 4 of the cell. Consequently, the derivatives at the corners are the least accurate, while the derivatives at internal points are the most accurate.

20. Numerical Example − Bubble Distributed Load on a Rectangular Plate

Here, the solution presented previously in **§13** is solved numerically. Only the upper right quadrant of the domain in Fig. 8 of that section is analyzed, owing to $x = 0$ and $y = 0$ being symmetry boundaries. The boundary conditions are

$$x = 0 \text{ and } y = 0 \;\Rightarrow\; \phi_t = \bar{V}_n = 0 \,, \qquad x = \frac{L}{2} \text{ and } y = \frac{H}{2} \;\Rightarrow\; u = \mathcal{M}_t = 0 \,. \tag{209}$$

Also, since $\phi_{t,t} = -u_{,nt} = 0$ on $x = 0$ and $y = 0$, $\mathcal{M}_n = 0$ so that the corner forces at the three corners excluding the upper right corner are known to be zero (the one at the upper right corner is unknown). The constants used in the calculation are

$$E = 3.0 \times 10^7 \text{ psi} \,, \quad \nu = 0.3 \,, \quad h = 1.0 \text{ in} \,, \quad L = 360 \text{ in} \,, \quad H = 240 \text{ in} \,, \quad F = 10000 \text{ lb} \,. \tag{210}$$

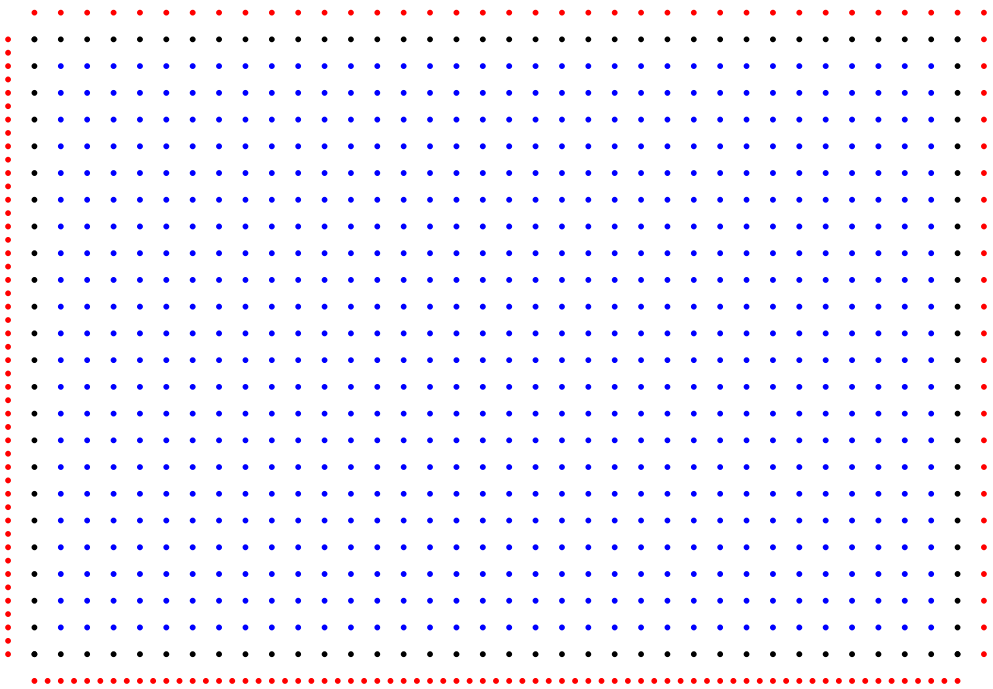

Figure 21. Computational grid used for the problem, as explained in the text.

The computational grid used is shown directly above in Fig. 21. The grid (excluding the red points) consists of an array of 36 by 24 points. The black points are on the boundary. Running between the black points are 116 boundary elements (the mid-point nodes 2 of each element are not shown, *cf.,* Fig. 11 of **§15**). The boundary points at the corners are double nodes, with adjacent boundary elements belonging to the two different faces of each corner. In the numerical solution, the continuity of the

displacement u at each double node is not enforced explicitly, but they do turn out to be continuous in the numerical solution (to 5 digits or so). The domain is filled with a 35 by 23 array of 805 integration cells, *cf.,* Figs. 16 and 17 of **§16**. Integrations along the boundary are carried out using the 16–point Gauss-Legendre rule, with the integration cells using 16 by 16 points. The 34 by 22 array of 748 blue points are in the interior of the domain, and these points are where the interior solution is calculated. The domain additionally is spanned by a 34 by 22 array of differentiation cells, *cf.,* Figs. 19 and 20 of **§18**, which cells are used to calculate the components of the shear vector **V** at both the black and blue points. Note that these cells overlap, so that each blue point corresponds to the central point 4 of a differentiation cell. Finally, the red points in the figure (outside of the domain of the plate) are where the singularities of the Green's functions are placed to generate equations for the unknown boundary values. The patterns of these points along the right and top faces correspond to the boundary condition case 2 of Fig. 13 in **§16**; while those along the left and bottom faces, to case 3 of Fig. 14 in **§16**. One additional red point is placed near the upper right corner (to generate an equation for the unknown corner force there).

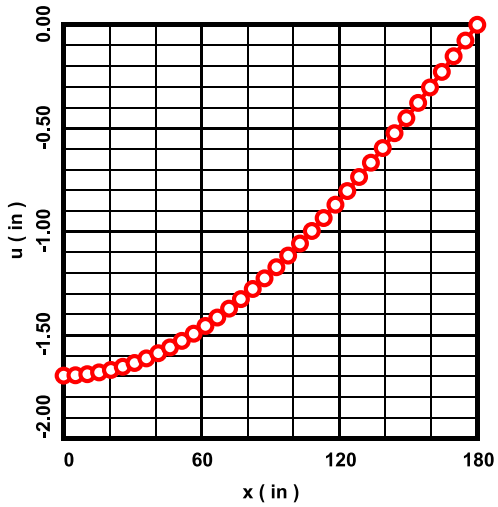

Figure 22. Numerical results for u at $y = 0$ compared to the exact solution.

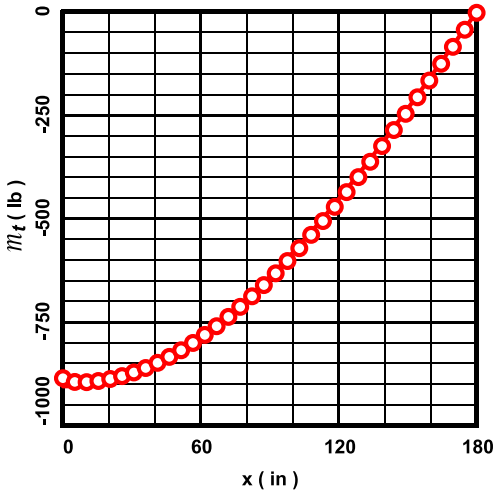

Figure 23. Numerical results for $\mathcal{M}_t$ at $y = 0$ compared to the exact solution.

Figures 22 and 23 above show the numerically calculated (open circles) and exact solution (solid lines) of the solved-for boundary values along the bottom face $y = 0$. The displacement u in Fig. 22 is highly accurate. The edge bending moment $\mathcal{M}_t$ in Fig. 23 is also very accurate, except that the numerical solution reaches its extremum at $x \approx 10$ in (as compared to $x = 0$ for the exact solution).

Figures 24 through 26 below show the results for, respectively, ϕ_y, M_{xy} and V_x along $y = 0$. The rotation in Fig. 24 $\phi_y = -\phi_n = -u_{,t}$ comes from nodal values of the boundary elements, and is highly accurate. The moment component M_{xy} in Fig. 25 is obtained from the boundary nodal-averaging technique described in **§17**, and it is also highly accurate. Finally, V_x in Fig. 26 is obtained by using the differentiation cells, as described in **§19**. While the values calculated for V_x are highly accurate for $15 \lesssim x \lesssim 170$ in, there is some inaccuracy near the boundaries. Specifically, there is a minor inaccuracy at $x \approx 170$ in, and for $0 \lesssim x \lesssim 15$ in, the numerical solution rises above the exact solution, although the absolute magnitude of the error is not substantial. Notwithstanding, these inaccuracies stem from the difficulty of finding third-order derivatives numerically, as will be discussed later in **§22**.

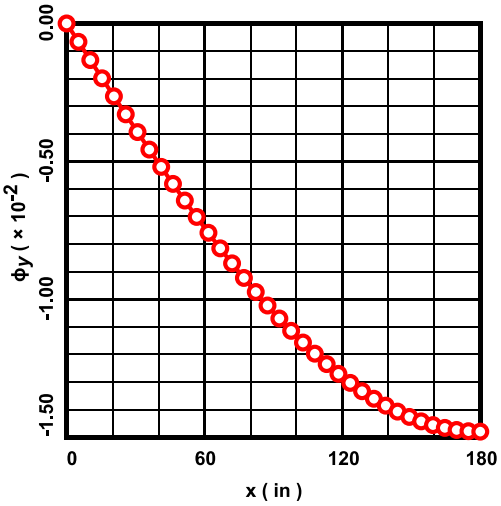

Figure 24. Numerical results for ϕ_y at $y = 0$ compared to the exact solution.

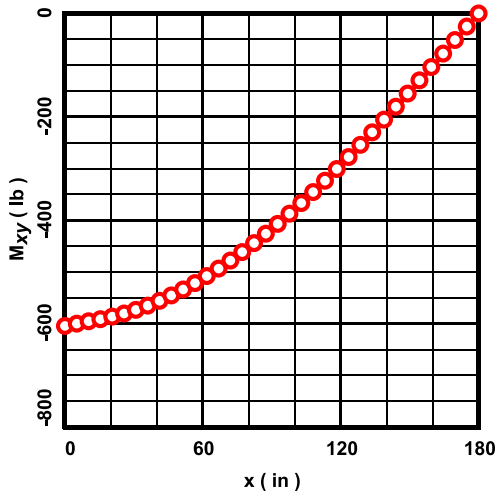

Figure 25. Numerical results for M_{xy} at $y = 0$ compared to the exact solution.

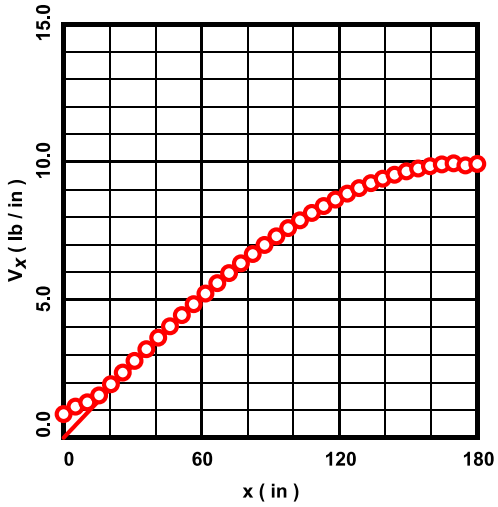

Figure 26. Numerical results for V_x at $y = 0$ compared to the exact solution.

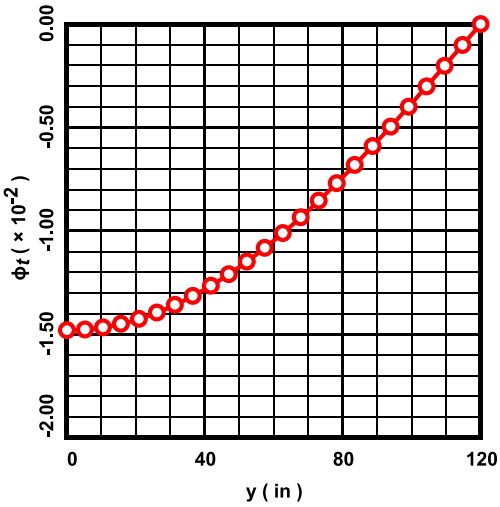

Figure 27. Numerical results for ϕ_t at $x = L/2$ compared to the exact solution.

Figure 27 above and Fig. 28 below show the solved-for boundary values, *i.e.,* ϕ_t and $\bar{V}_n$ respectively, on the right face $x = L/2$ of the domain. These numerical results are highly accurate.

Figures 29 and 30 below show the results for, respectively, M_{xx} and V_x, also on the face $x = L/2$. The numerical calculation of the twisting moment M_{xx} is, again, highly accurate, which follows from the fact that M_{xx} is proportional to boundary element nodal values. The numerical results for V_x in Fig. 30 are also accurate, except for the slight inaccuracy near the boundary for $0 \lesssim x \lesssim 5$ in.

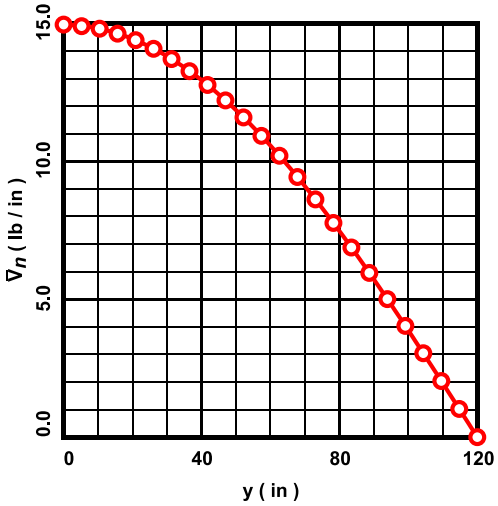

Figure 28. Numerical results for $\bar{V}_n$ at $x = L/2$ compared to the exact solution.

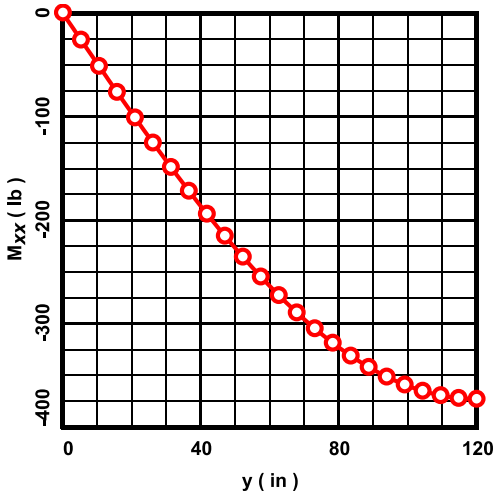

Figure 29. Numerical results for M_{xx} at $x = L/2$ compared to the exact solution.

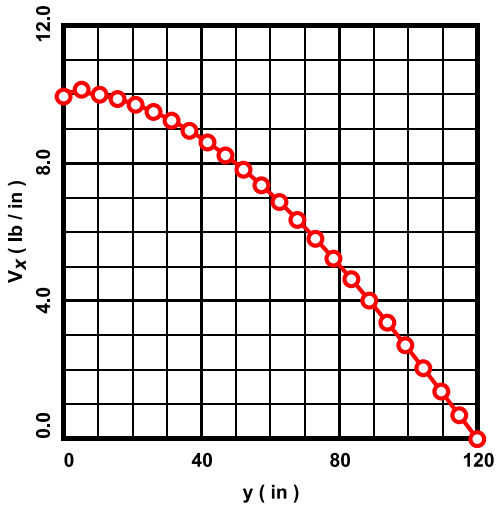

Figure 30. Numerical results for V_x at $x = L/2$ compared to the exact solution.

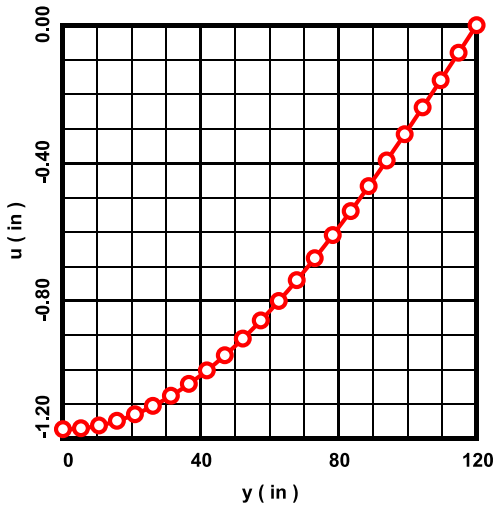

Figure 31. Numerical results for u at $x = 92.5714$ in compared to the exact solution.

Figure 31 above and Figs. 32 through 34 below show the numerical results along a vertical line through the domain located approximately mid-way between the left and right boundaries. Once again, from Fig. 31, the numerically calculated displacement u is very accurate, as are the calculated components of the rotation vector $\boldsymbol{\phi}$ in Fig. 32. The calculated components of the moment tensor $\mathbf{M}$ in Fig. 33, additionally, are very accurate. Finally, the numerically calculated components of the shear vector $\mathbf{V}$ in Fig. 34 are accurate, except for the inaccuracy in V_y near the boundary at $0 \lesssim x \lesssim 10$ in.

The last numerical result concerns the corner force at the upper right corner. To the nearest tenth, the exact value of the force is -745.6 lb, while the numerically calculated value is -745.1 lb.

All in all, except for near the boundary in some cases, with regard to the shear vector **V**, the numerical method produces highly accurate results.

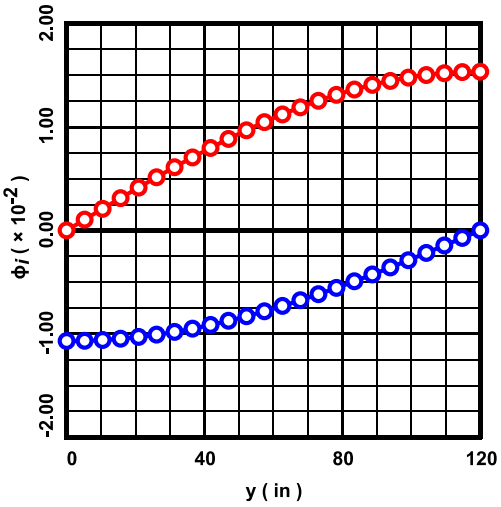

Figure 32. Numerical results for ϕ_x (red) and ϕ_y (blue) at $x = 92.5714$ in compared to the exact solution.

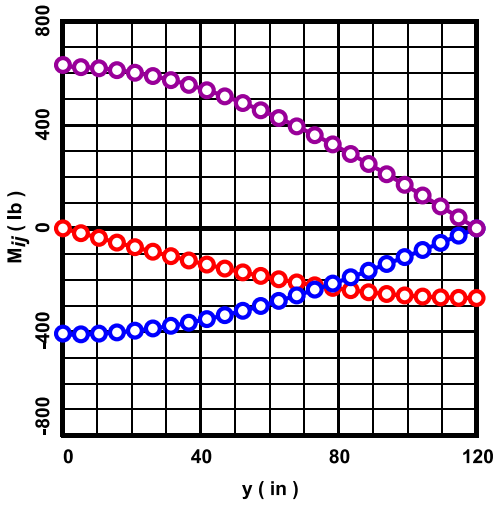

Figure 33. Numerical results for M_{xx} (red), M_{xy} (blue) and M_{yx} (purple) at $x = 92.5714$ in compared to the exact solution.

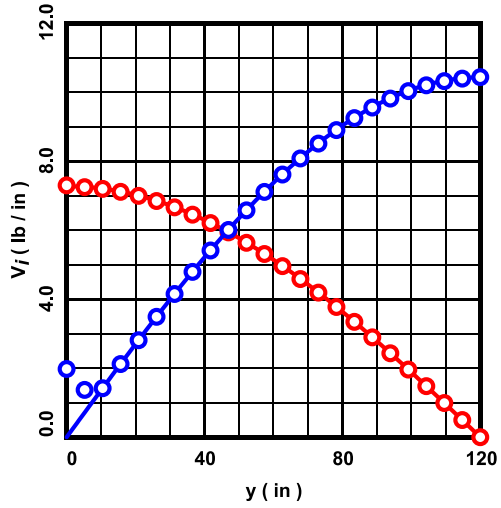

Figure 34. Numerical results for V_x (red) and V_y (blue) at $x = 92.5714$ in compared to the exact solution.

21. Numerical Example – Sinusoidal Transverse Edge Load on an Annular Cantilever Plate

Here, the problem solved analytically in **§14** is solved numerically. The boundary conditions for the problem were given previously by eqns. (147) through (149) of §**14**, and the constants used were given by eqn. (159).

The computational grid used for the analysis is shown below in Fig. 35. As was the case previously in **§20**, the black points are on the boundary of the domain, the blue points are in the interior of the domain, and the red points are outside of the domain. Excluding the red points, the grid is a 25 (radial) by 35 (tangential) array of points, making for 116 boundary elements, 759 interior points, and 759 differentiation cells. Like in Fig. 21 of **§20**, the boundary elements run between the black points, and their mid-nodes (*i.e.,* node 2, *cf.,* Fig.11 of **§15**) are not shown. Also, as previously, the black nodes on the corners are double nodes. Since there is no distributed load, there are no integration cells. Once again, the red points in the figure are where the singularities $\mathbf{x}^0$ of the Green's functions are placed to generate equations for the unknown boundary values (and corner forces). The pattern of the red points at the inner radius $r = a$ correspond to the boundary condition case 1 (Fig. 12 in **§16**); the pattern at the faces $\theta = 0$ and $\theta = \pi/2$, to

case 2 (Fig. 13 in **§16**); and finally, the pattern at the outer radius $r = b$, to case 4 (Fig. 15 of **§16**). The corner forces on the inner radius are known to be zero, and the two red points near the outer radius at $\theta = 0$ and $\theta = \pi/2$ generate equations for the unknown corner forces at those two points. Note that these two red points are not symmetrically placed. While the author finds this to be quite curious, if these two points are symmetrically placed, then the resulting system of equations is singular (rank 429 out of 430 equations). Nonsymmetric placement yields full rank. In any case, the boundary integrations are carried out using the 32–point Gauss-Legendre quadrature rule.

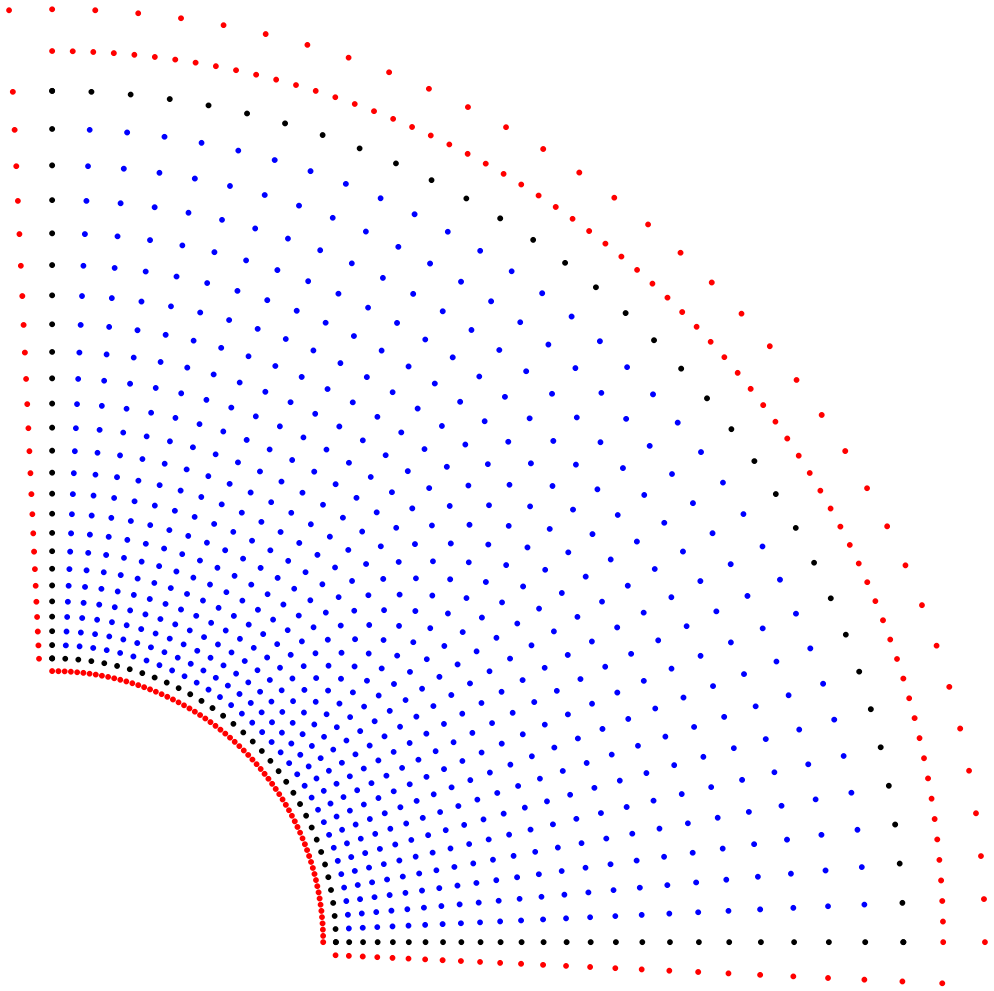

Figure 35. Computational grid for the problem as explained in the text.

Figures 36 and 37 below show the numerically calculated results (plotted points) compared to the exact solution (solid lines) for the solved-for boundary values on the face $\theta = 0$. As seen from Fig. 36, the numerical results for the rotation ϕ_t are highly accurate. Figure 37 gives the results for $\bar{V}_n$, which can be seen is also very accurate (except near the outer radius at $340 \lesssim r \lesssim 360$ in, where there is some minor error).

Figures 38 and 39 below give the results for, respectively, the solved-for boundary values u and ϕ_t on the face at the outer radius $r = b$. Both results, *i.e.,* u and ϕ_t, are highly accurate.

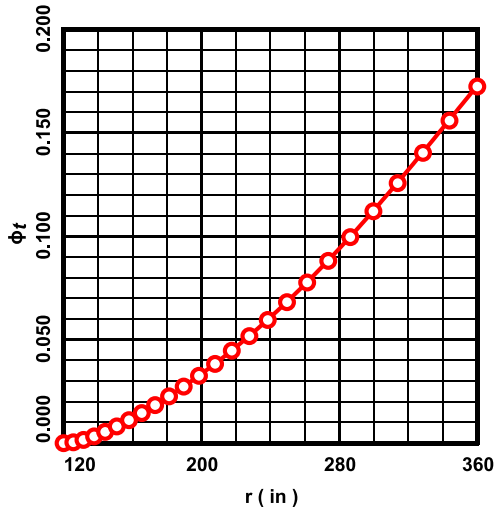

Figure 36. Numerical results for ϕ_t at $\theta = 0$ compared to the exact solution.

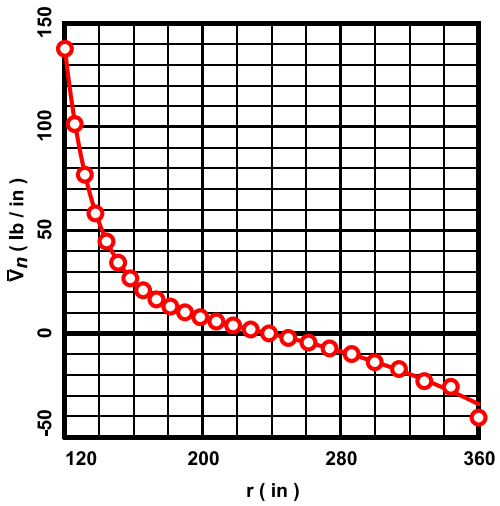

Figure 37. Numerical results for $\bar{V}_n$ at $\theta = 0$ compared to the exact solution.

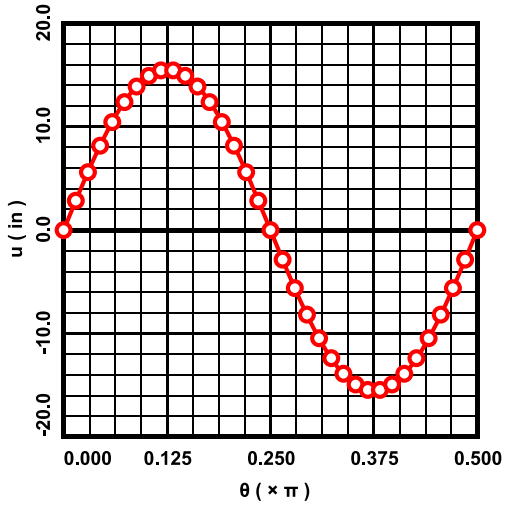

Figure 38. Numerical results for u at $r = b$ compared to the exact solution.

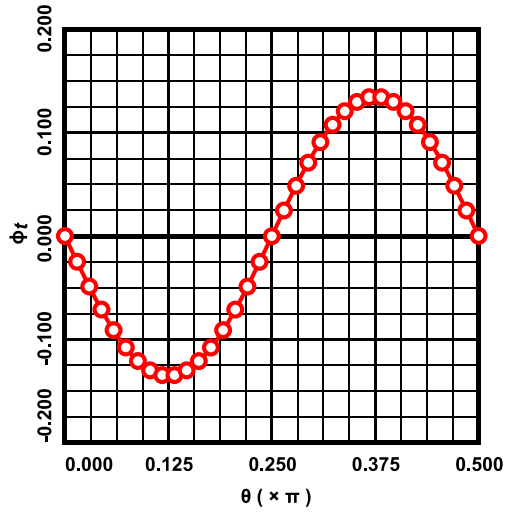

Figure 39. Numerical results for ϕ_t at $r = b$ compared to the exact solution.

Figures 40 and 41 below show the results for the solved-for boundary values $\mathcal{M}_t$ and $\bar{V}_n$, respectively, on the inner radius $r = a$. From Fig. 41, one sees that the results for $\mathcal{M}_t$ are highly accurate. From Fig. 41, while the absolute magnitudes of the calculated values of $\bar{V}_n$ are quite accurate, there is some small amount of oscillation present in the results, which indicates possibly that the system of equations is slightly ill-conditioned. Nevertheless, an initial attempt at solving this problem with the straight-line version of the boundary element of **§15** gave highly inaccurate results for $\bar{V}_n$. Thus, the use of curved boundary elements is an absolute necessity.

Corner force at (r, θ)	Exact value (lb)	Numerically calculated value (lb)	Relative error (%)
$(b, 0)$	-3935.94	-3893.54	-1.08
$(b, \pi/2)$	3935.94	4005.38	1.76

Finally, concerning the solved-for boundary values, the table directly above shows the values of the exact and numerically calculated non-zero corner forces. As is evident, the numerical values are not exactly anti-symmetric (as they should be). This probably is because of the (necessarily) non-symmetric placement of the red (singularity) points for these corner forces, as was described above concerning Fig. 35. Also, perhaps again, this is due to a possibly ill-conditioned system. Notwithstanding, the relative error of the numerical results is acceptably small.

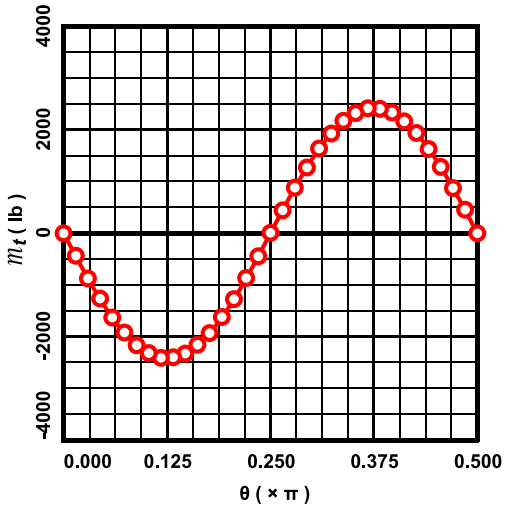

Figure 40. Numerical results for $\mathcal{M}_t$ at $r = a$ compared to the exact solution.

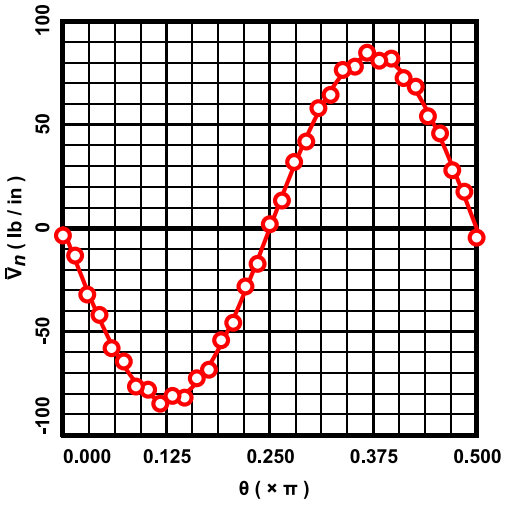

Figure 41. Numerical results for $\bar{V}_n$ at $r = a$ compared to the exact solution.

Figures 42 through 45 below show the calculated results for the tensorial quantities along a radial line of points through the domain of the plate located at $\theta = 9\pi/68 \approx 23.83°$. As Figs. 42 and 43 show, respectively, the calculated results for the displacement u and rotation vector $\boldsymbol{\phi}$ are highly accurate.

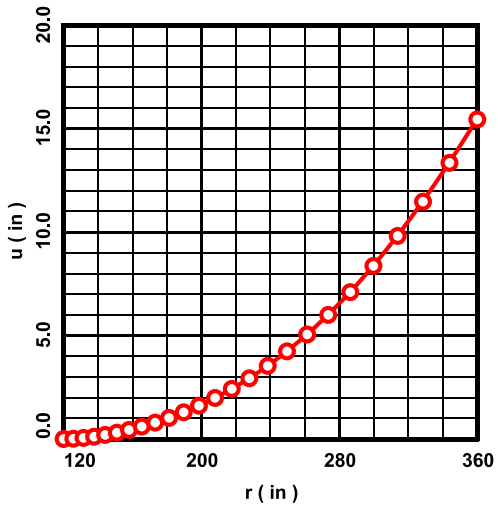

Figure 42. Numerical results for u at $\theta \approx 23.83°$ compared to the exact solution.

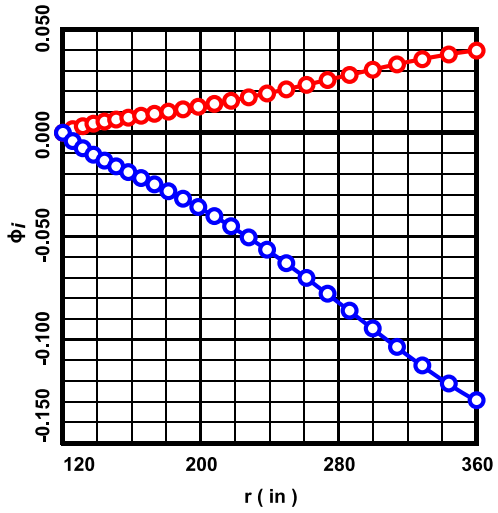

Figure 43. Numerical results for ϕ_x (red) and ϕ_y (blue) at $\theta \approx 23.83°$ compared to the exact solution.

Concerning the results for the moment tensor **M**, as per Fig. 44, once again the numerical results are highly accurate, except for small inaccuracies at the outer radius $r = b = 360$ in for the components M_{xx} and M_{xy}. Finally, Fig. 45 gives the results for the shear vector **V**. For $0 \leq r \lesssim 330$ in, the numerically calculated values of V_i are accurate. But, as one approaches the outer radius of the domain, the results exhibit fairly significant error (especially V_y).

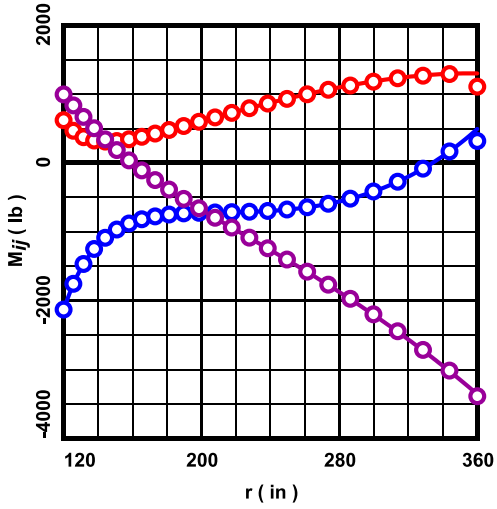

Figure 44. Numerical results for M_{xx} (red), M_{xy} (blue) and M_{yx} (purple) at $\theta \approx 23.83°$ compared to the exact solution.

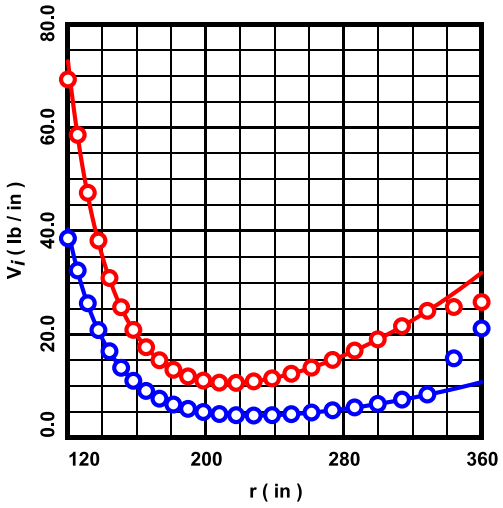

Figure 45. Numerical results for V_x (red) and V_y (blue) at $\theta \approx 23.83°$ compared to the exact solution.

For the circular arc of grid-points located at $r = 207.8461$ in, Figs. 46 through 49 below present the results for the tensorial quantities. The numerical results for the displacement u, the rotation vector $\boldsymbol{\phi}$

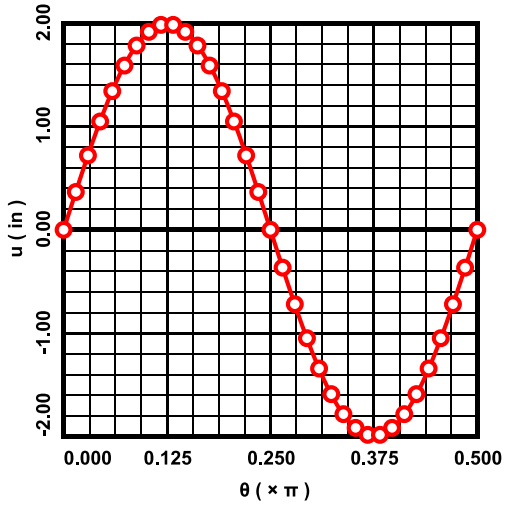

Figure 46. Numerical results for u at $r = 207.8461$ in compared to the exact solution.

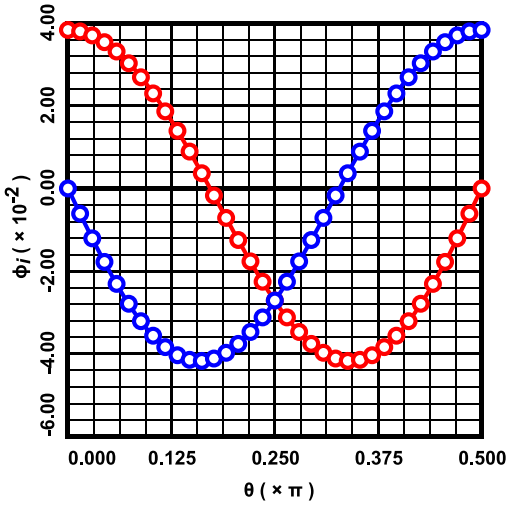

Figure 47. Numerical results for ϕ_x (red) and ϕ_y (blue) at $r = 207.8461$ in compared to the exact solution.

the moment tensor **M**, and the shear vector **V**, as seen from Figs. 46 through 49 respectively, all are highly accurate.

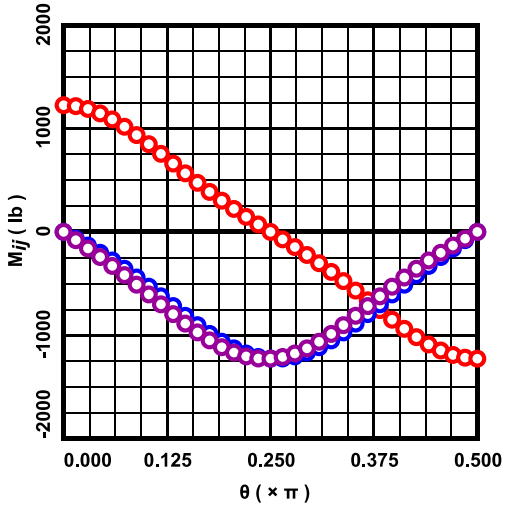

Figure 48. Numerical results for M_{xx} (red), M_{xy} (blue) and M_{yx} (purple) at $r = 207.8461$ in compared to the exact solution.

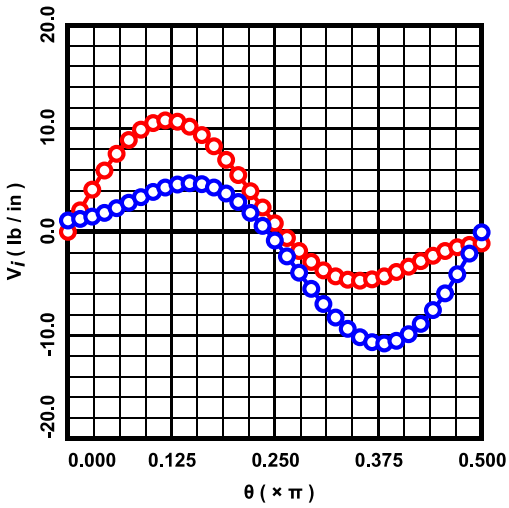

Figure 49. Numerical results for V_x (red) and V_y (blue) at $r = 207.8461$ in compared to the exact solution.

22. Closing Comments

Here, a few things learned by the author, during performing this work, are discussed. First, if the plate has curved boundaries, then the use of curved boundary elements is required to obtain accurate solutions.

The orders of interpolations used for the boundary values of u, ϕ_t, $\mathcal{M}_t$ and $\bar{V}_n$ must decrease by one each time, like in **§15**, where the orders, respectively, are 4, 3, 2 and 1. If this is not done, then either oscillatory solutions are obtained, or smooth solutions which do not converge to the correct results are obtained.

The biggest difficulty is the calculation of accurate values of the components of the shear vector **V**, especially on the boundary. If more accurate values of **V** on the boundary can be obtained, then the differentiation cells of **§19** would only need to be used at interior points, which would be more accurate. One possibility for obtaining more accurate values of **V** on the boundary would be to employ higher order interpolations in the boundary element, so that all the components of the moment **M** (or even all the components of both **M** and **V**) would be continuous on the boundary. Higher order interpolations, though, would yield more degrees-of-freedom per element, and would require the use of more singularity points than shown in Figs. 12 through 15 of **§16**.

Finally, it appears that using the fourth of eqns. (197) and (198) of **§18** to calculate **V** in the interior, as opposed to using the differentiation cells, requires that the calculated boundary values be extremely accurate. Perhaps higher order interpolations in the boundary element would help in this regard.